Nanoscale Advances

REVIEW

View Article Online
View Journal | View Issue

Cite this: *Nanoscale Adv.*, 2022, **4**, 3689

Polyoxometalate-based nanocomposites for antitumor and antibacterial applications

Dening Chang, Yanda Li, Yuxuan Chen, Xiaojing Wang, Dejin Zang and Teng Liu *

Polyoxometalates (POMs), as emerging inorganic metal oxides, have been shown to have significant biological activity and great medicinal value. Nowadays, biologically active POM-based organic–inorganic hybrid materials have become the next generation of antibacterial and anticancer drugs because of their customizable molecular structures related to their highly enhanced antitumor activity and reduced toxicity to healthy cells. In this review, the current developed strategies with POM-based materials for the purpose of antibacterial and anticancer activities from different action principles inducing cell death and hyperpolarization, cell plasma membrane destruction, interference with bacterial respiratory chain and inhibiting bacterial growth are overviewed. Moreover, specific interactions between POM-based materials and biomolecules are highlighted for a better understanding of their antibacterial and anticancer mechanisms. POMs have great promise as next-generation antibacterial and anticancer drugs, and this review will provide a valuable systematic reference for the further development of POM-based nanomaterials.

Received 18th June 2022
Accepted 17th August 2022

DOI: 10.1039/d2na00391k

rsc.li/nanoscale-advances

1. Introduction

The development of anticancer and antimicrobial agents is a significant challenge for public health worldwide. In recent decades, due to the changes and pollution in the people's living environment, the incidences of cancer have been increasing year by year, showing increasing population being affected at a younger age. The World Health Organization reports that cancer is the leading cause of death worldwide, accounting for nearly 10 million deaths by 2020.[15] The causative factors of cancer are personal genetic factors and external factors (physical factors, chemical factors, and biological factors), in which biological factors include infection with certain viruses, bacteria, or parasites. In recent years, the emergence of some drug-resistant bacteria has also made the treatment of infections challenging.[14] Therefore, there is an urgent need to develop new antitumor and antimicrobial agents to accurately discover and effectively treat the diseases we face.

Polyoxometalates (POMs) are metal–oxygen clusters formed by covalently linking transition metal elements (Mo, W, V, Nb, and Ta) with oxygen atoms.[18–20] By virtue of their structural diversity and redox chemical properties, POMs and their composites have been proved to have great biomedical potential

Institute of Materia Medica, Shandong First Medical University & Shandong Academy of Medical Sciences, Jinan, 250117, PR China. E-mail: liuteng823@163.com

Dening Chang is studying for his Master's degree at Shandong First Medical University & Shandong Academy of Medical Sciences, China. His research interest is the pharmacological activities of polyoxometalates-based nanocomposites.

Yanda Li is a research assistant in Shandong First Medical University & Shandong Academy of Medical Sciences, China. His current research is in the self-assembly of polyoxometalates.

and have been widely studied and applied in the medical field (Fig. 1). In 1965, the *in vivo* antitumor activity of POMs was first reported, with a combination of $H_3[PW_{12}O_{40}]$, $H_3[PMo_{12}O_{40}]$ and caffeine in patients with gastrointestinal cancer. In 1970, Chermannet *et al.* detected the inhibitory effect of silowolic acid on mouse leukemia and sarcoma viruses, revealing the inhibitory effect of POMs on enzymes, and thus began the systematic study of its antiviral effect.[21] In addition, the antimicrobial activity was also reported, which is of great significance in the fight against drug-resistant bacteria.[22,23] There is also the effect of insulin mimicking to control diabetes,[24] as well as Alzheimer's disease.[25] However, some disadvantages of pure inorganic POMs, such as high toxicity and long-term toxicity, limit their scope of clinical application. Therefore, with the development of nanotechnology and materials science, the research on POMs is no longer limited to pure inorganic POMs but also includes POM-based nanohybrid compounds, which can reduce the toxicity of POMs and improve the structural stability of POMs through functional combination or encapsulation of organic structures, and even develop related products with more functions.[26,27] Due to the specificity of POM structures, the shell of POMs carries a large amount of negative charge.[28] This surface feature results in strong ionic interactions when mixed with cations, wherein electrostatic interactions are the main driving force.[29] When combined with organic cations (such as cationic surfactants,[30,31] amino acids,[32] peptides,[33] and proteins[34,35]), the POM matrix size, polarity, and surface charge properties can be changed to obtain a new complex. She *et al.* developed a degradable aliphatic organoimido derivative that exhibited promising pharmacodynamic properties against human malignant glioma cells (U251), and its toxicity to normal cells was reduced after degradation, which paved a new pathway for the construction of degradable anticancer agents. Their study also confirmed that the DCC-dehydration protocol could be an effective method for covalently grafting bioactive ligands such as amantadine to POMs and strengthen their application in cancer therapy.[36,37] Gu *et al.* obtained supramolecular assemblies by the self-assembly of iodobodipy with POMs, which can be applied to photodynamic therapy (PDT) to kill cancer cells.[38] Such organic modified composite materials can increase the stability, biocompatibility, and cell permeability, reduce the toxicity, and achieve better antibacterial effects.

In this paper, the development direction of polyoxometalates for antibacterial and anticancer purposes in recent years is reviewed in terms of inducing cell hyperpolarization and death, destroying cell membranes, interfering with the bacterial respiratory chain, inhibiting bacterial growth, and cell imaging techniques. In addition, the special interactions between POM-based materials and biomolecules are highlighted in order to better understand their related antibacterial and anticancer mechanisms. This paper reviews the latest research progress of polyoxometalates in antitumor and antibacterial aspects,

Yuxuan Chen is a research assistant in Shandong First Medical University & Shandong Academy of Medical Sciences, China. His current research is on the pharmacological activities of polyoxometalates.

Dejin Zang obtained his PhD degree from University of Strasbourg in 2017. He is working as an associate professor at Shandong First Medical University & Shandong Academy of Medical Sciences, China. His research interest is in the application of transition metal oxide clusters-based functional materials in electrocatalysis.

Xiaojing Wang is a professor at Shandong First Medical University & Shandong Academy of Medical Sciences, China. She is the Executive Vice President of the School of Pharmacy and Pharmaceutical Sciences. Her research interests are in the synthesis and structural modification of active ingredients.

Teng Liu obtained her PhD degree from Shandong University in China in 2013. She has been working at Shandong First Medical University & Shandong Academy of Medical Sciences, China. Her research interests are the self-assembly of amphiphilic molecules and their related applications in biology and medicine.

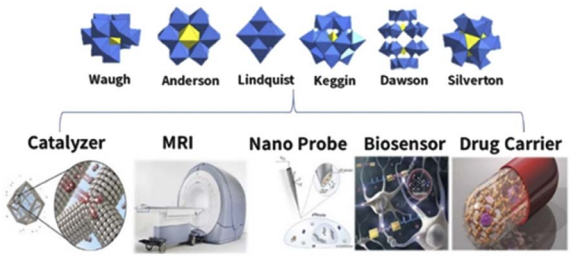

Fig. 1 Typical structure and application of polyoxometalates.

providing a reference for the rational design of a new generation of biological drugs.

2. Application of polyoxometalates in anticancer therapy

Cancer is caused by a variety of factors; chemotherapy, radiotherapy, and surgery are the conventional treatments of cancer at present. Among them, chemotherapy is the most common method. Among chemotherapeutic drugs, cisplatin (CDDP) is the most prominent cytotoxic drug, which is still one of the most widely used chemotherapeutic drugs in clinic. In addition to CDDP, a range of other drugs cure cancer by temporarily relieving symptoms, prolonging patients' lives, and even, in rare cases, curing cancer.[39,40] However, due to the lack of selectivity and serious side effects, the treatment efficiency and bioavailability of some cancers are low. Thus, the search is still on for alternative drugs that selectively incapacitate cancer cells without seriously damaging normal ones. POM-based nanocomposites have become a hot research topic due to their excellent properties, and thus a variety of diagnostic and therapeutic methods have been born.

2.1 Nanoprobes

Cellular signaling molecules, such as metal ions, reactive oxygen species (ROS), and active nitrogen substances (RNS), are closely related to various physiological and pathological processes.[41,42] Therefore, the efficient detection of small cell molecules is of great significance for disease diagnosis and human health management. Among them, the excessive production of hydrogen peroxide (H_2O_2) in reactive oxygen species (ROS) is related to the generation of many inflammatory diseases; thus, the detection of H_2O_2 has become a research hotspot.[43] In addition, it can also indicate the emergence of a variety of human diseases, including neurodegenerative disorders and cancer, which has good application prospect in cancer monitoring and diagnosis.[44–46] At present, the most commonly used H_2O_2 detection method is horseradish peroxidase (HPR), which catalyzes the oxidation of H_2O_2 to form colored products. However, HPR also has disadvantages, such as high production cost and instability in extreme conditions, which limit its application.[47] In recent years, POMs have been proved to be an artificial enzyme to simulate natural peroxidase in the determination of H_2O_2, as shown in Table 1. In 2012, Wang *et al.*[48] found three polyoxometalates ($H_3PW_{12}O_{40}$, $H_4SiW_{12}O_{40}$, and $H_3PMo_{12}O_{40}$) and found that these three polyoxometalates have peroxidase activity and can catalyze 3,3′,5,5′-tetramethylbenzidine (TMB) oxidation by H_2O_2 to show a blue color. Among them, the catalytic activity of $H_3PW_{12}O_{40}$ was higher than that of HPR. This finding creates a better way to detect H_2O_2.

The biocompatibility of POMs and their ability to target cancer cells are two optimization directions to improve their performance. Taking advantage of the overexpression of folic acid receptor in human tumor cells, Wu's group[50] constructed FA-functionalized phosphovanadomolybdate (PMV), which promotes the oxidation of TMB at neutral pH without an oxidizing agent due to its unique oxidase-like activity. Based on the principle of mutual recognition between folate and the folate receptor, the FA-PMV complex showed sensitive detection response to folate receptor overexpression human hepatocellular liver carcinoma cell line (HepG2), hamster ovary cells (CHO), and human breast cancer (MDA-MB-231), demonstrating the excellent ability to target cancer cells.

However, the poor dissolvability of folic acid seriously limits its copolymerization with POMs. Therefore, Ma *et al.*[10]

Table 1 Overview of POM composites mentioned in this paper as artificial enzymes to simulate peroxidase[a]

POM composite	Main findings	Application	Ref.
FA-γ-[$(FeOH_2)_2SiW_{10}O_{36}$] (abbr. FA-$SiW_{10}Fe_2$)	Facilitate the combination and oxidation of TMB with H_2O_2	Colorimetric immunoassay	49
$K_5PV_2Mo_{10}O_{40}$-FA (abbr. PMV-FA)	Catalytic oxidation of cancer cells and sensitive colorimetric substrates (TMB) based on folic acid	Colorimetric immunoassay	50
$PMo_{12-n}V_nO_{40}$-FA_n (abbr. PMoVn-FA)	The activity of oxidase changed with the vanadium content	Colorimetric immunoassay	51
$[Ag_3(FKZ)_2(H_2O)_2][H_3SiW_{12}O_{40}]$ @PPy (abbr. AgFKZSiW_{12}@PPy)	Synergistic improvement of peroxide-like enzyme activity, rapid reaction, and reduction of LOD for H_2O_2 and AA	Colorimetric immunoassay and medical diagnosis	52
$(NH_4)_5H_6PMo_4V_8O_{40}$-FA (abbr. PMo_4V_8-FA)	H_2O_2 and sarcosine in real urine were detected without SOD	Colorimetric detection of sarcosine	16

[a] FA: folic acid; TMB: 3,3′,5,5′-tetramethylbenzidine; AA: ascorbic acid; SOD: ascorbic acid; LOD: limit of detection.

constructed a new composite material to solve this problem. Through the electrostatic interaction between the cations and POMs, $H_3PW_{12}O_{40}$ (PW_{12}) was encapsulated by diphenylalanine peptide (L-Phe-L-Phe) (FF). Among them, FF can improve the biocompatibility and affinity for TMB through non-covalent interaction. Graphene oxide (GO) was then co-assembled with the prepared microspheres to prepare a ternary hybrid structure, $FF/PW_{12}/GO$ (Fig. 2A), which showed GO-modified peroxidase-like performance through hydrogen bonding and ion interactions with POMs.

The folate-functionalized polyoxometalate (PMO_4V_8-FA) mentioned in Table 1 also showed strong peroxidase-like activity.[16] Through comparative experiments (Fig. 2C), PMO_4V_8-FA oxidizes TMB in the absence of H_2O_2, showing oxidation-like properties, and the blue solution produced by PMO_4V_8-FA produces an absorbance peak at 652 nm. Due to the presence of PMO_4V_8-FA, H_2O_2 greatly improves the oxidation capacity of TMB, and the presence of O_2 does not affect the detection results of H_2O_2. The peroxidase activity of PMO_4V_8-FA was concentration-dependent (Fig. 2B) and varied with the concentration of TMB (0.025–0.08 mM). It also has the ability to detect sarcosine, which is a biomarker of prostate cancer. The sensitivity of this double marker is of great significance for inchoate detection and diacrisis of prostate cancer. The modification of these biocompatible molecules enhanced the potential of POMs as a nanoprobe to detect H_2O_2. It also points the way for future research and raises the prospect of cancer prevention and surveillance.

Glutathione (GSH), which plays a role as an antioxidant in cells, is the most abundant small molecular weight cysteine-containing thiols in cells.[53] GSH can prevent cellular component damage caused by oxidative stress, and excessive GSH in cancer cells can lead to resistance to radiotherapy/chemotherapy and promote tumor invasion/metastasis.[54,55] By reducing GSH in cancer cells, the effect of chemoradiotherapy can be increased, and the resistance to oxidative stress can be reduced, thereby accelerating apoptosis. The mechanism can be used not only for anticancer but also for anti-infection to accelerate bacterial death, which we will discuss in the antibacterial part. Therefore, GSH-related diseases can be accurately diagnosed earlier by the detection and quantification of GSH levels.

Chen's group reported a new ratiometric GSH-specific nanoprobe that formed uniform nanoparticles(CR-POM) by self-assembling synthetic croconaine (CR) dye and molybdenum (Mo)-based polyoxometalate clusters (Fig. 3).[1] It was found by the study that the CR dye can be specifically reduced by GSH, showing a distinct GSH concentration-dependent decrease in the absorbance at 700 nm. Since the CR dye is electrophilic, its electron-deficient central five-membered ring is highly vulnerable to nucleophilic attack by thiols, and leads to an abrupt decrease in the NIR absorbance. On the other hand, GSH can reduce Mo-based POM clusters to increase their absorbance at 866 nm due to GSH-activated Mo(VI) to Mo(V) conversion. The increase in POM reduction promotes the delocalized electron density and occupation of the cation position of Mo(V) through reversible multistep electron exchange, which leads to enhanced electron relaxation polarization and NIR absorption (Fig. 3A). Moreover, the NIR absorbance of POMs at 866 nm showed GSH concentration dependence (Fig. 3B). More importantly, the acidic tumor microenvironment (TME) can induce hydrogen bonds through the protonation of POM clusters to drive the self-assembly and aggregation of CR-POM, allowing the conversion of CR-POM from small nanoparticles (105 nm) to large particles (1–2 μm), which facilitates prolonged intratumoral residence time and amplifies its PA signals (Fig. 3C). Excessive GSH in the tumor can make the PA_{866} signal become stronger, while the PA_{700} signal gets weaker, which will provide a large PA_{866}/PA_{700} ratio. Therefore, the PA signal ratio of CR-POM at these two wavelengths is much higher than that of most existing ratiometric PAI probes, which endows these nanoparticles with ultra-high

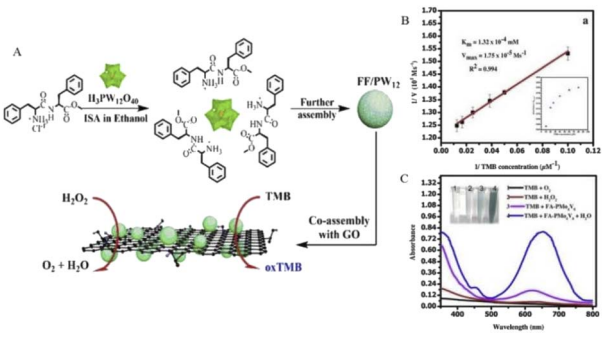

Fig. 2 (A) FF/PW_{12}/GO construction diagram. Copied with permission.[10] Copyright 2015, American Chemical Society. (B) Steady-state kinetic study of oxidation of TMB by PMO_4V_8-FA. (C) PMO_4V_8-FA showed peroxidase-like activity when TMB was oxidized at room temperature for 2 min under the conditions of TMB (0.08 mM), PMO_4V_8-FA (0.024 mM), and H_2O_2 (0.15 mM). Copied with permission.[16] Copyright 2020, with permission from Elsevier.

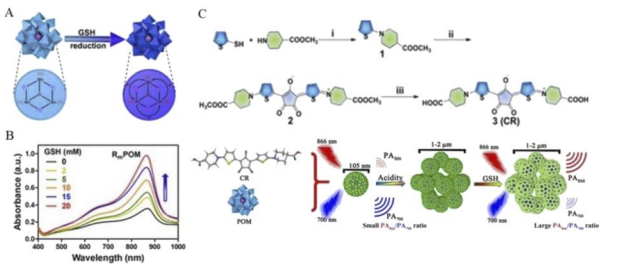

Fig. 3 (A) GSH activates POMs, in which the oxidation state of Mo(VI) is converted to Mo(V). (B) The NIR absorbance of POM at 866 nm showed a concentration-dependent increase in GSH. (C) CR was synthesized by a three-step method. First, compound 1 was obtained by a nucleophilic substitution reaction between thiophene-2-thiol and amino group. Then, compound 2 was synthesized by the condensation reaction of 2 equivalents of compound 1 with croconic acid, and the final product CR was obtained by ester hydrolysis. CR then produced a concentration-dependent response to GSH after assembly with POMs into nanoprobes to obtain PA signal values.[1] Copyright 2019, with permission from American Chemical Society.

detection sensitivity for GSH so as to achieve high accurate detection and quantification of GSH levels in tumors.

It was also found that CR dyes can be radiolabeled by chelation with ^{64}Cu and experimentally found to be suitable for *in vivo* positron emission tomography (PET) imaging in mouse serum and tumor-bearing mice. This also allows quantitative drug imaging to monitor the whole-body distribution of CR-POM nanoprobes *in vivo* by positron emission tomography imaging. The advent of this multifunctional and highly sensitive nanoprobe provides a new method for early diagnostic research of tumors and a platform for the accurate diagnosis of other GSH-related biological processes and diseases.

2.2 Biosensors

Biosensor analytical devices can be used to detect specific biological analytes. Specific biomarkers will be generated when cancer appears. Therefore, the efficient detection of cancer cells through biosensors is crucial in early cancer diagnosis and clinical research, and can effectively improve the survival rate of cancer patients.[32,56,57]

The development of biosensors that use POMs to detect cancer biomarkers began in 2011. Current studies have used a similar strategy to interact with the cell-specific overexpression of folate receptors through folate–folate receptor interactions. Then, the chromaticity signal was affected through the activity of oxidase, and the dye 3,3′,5,5′-tetramethylbenzidine (TMB) was further oxidized to cause the blue reaction.[58,59] Although currently-developed POM biosensors for folic acid have shown promising results, the specificity of cancer cells cannot be guaranteed by a single assay. Therefore, to ensure the precision of cancer cell detection, it is necessary to develop detection methods for different cell analytes.

Osteopontin (OPN) is a multifunctional phosphoglycoprotein that is expressed in a variety of cells, including osteoclasts, osteoblasts, myeloid cells, and innate lymphocytes. In patients with cancer, especially gastric cancer and liver cancer, the overexpression of OPN is often detected in the tumor microenvironment, and elevated serum OPN levels are associated with poor prognosis.[9,60,61] This relationship can be used to correlate the prognosis of cancer with detection.

In a recent study, Zhou *et al.*[9] reported a complex PPy@Ti_3C_2Tx/PMo_{12}. PMo_{12} has rich electrochemical properties and can carry out reversible multi-step and multi-electron transfer; thus, it can be used as electrochemical transducers. Meanwhile, $Ti_3C_2TxMXene$, PMo_{12}, and PPy have good biocompatibility, good electrochemical activity, and strong bioaffinity to biomolecules.[62,63] The nanohybrid Ti_3C_2Tx/PMo_{12} was composed of phosphomolybdic acid (molybdic acid) (PMo_{12}) and $Ti_3C_2TxMXene$, then wrapped by polypyrrole (PPy) layers (represented by PPy@Ti_3C_2Tx/PMo_{12}) (Fig. 4). Subsequently, a large number of OPN RNA aptamers were fixed on the surface of the PPy@Ti_3C_2Tx/PMO_{12} complex through π–π stacking, electrostatic interaction, and hydrogen bonding to construct the electrochemical aptamer sensor. As can be seen from Fig. 4, when OPN exists, a G-quadruplex is formed between OPN and the OPN aptamer chain as a result of its specific recognition,

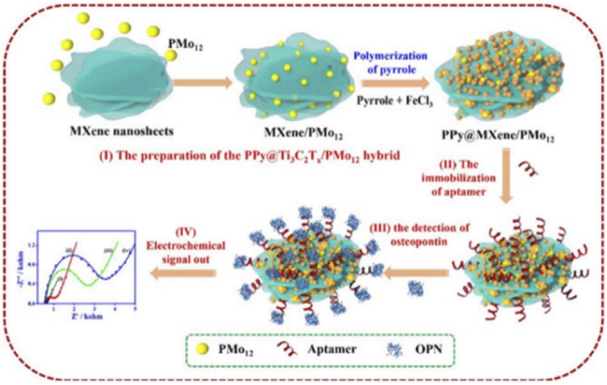

Fig. 4 PPy@Ti_3C_2Tx/PMo_{12} sensor fabrication and working process diagram. Copied with permission.[9] Copyright 2019, with permission from Elsevier.

and then the conformation of the aptamer chain changes, causing steric hindrance. This change can be monitored by electrochemical methods (such as electrochemical impedance spectroscopy) with a low detection limit (0.98 fg mL^{-1}). Because there is no such specific interaction between OPN aptamers and other cancer markers or interferents, the PPy@Ti_3C_2Tx/PMO_{12} sensor shows excellent selectivity for OPN. It also provides an alternative approach for the detection of tumor markers, in which multi-site detection of cancer cells can effectively improve the success rate and accuracy of early cancer diagnosis. This can lead to earlier detection and earlier treatment for patients.

2.3 Magnetic resonance imaging

Rapid developments in accurate medicine and life science require precise diagnosis at the levels of cells, tissues, organs, and human bodies. With the deepening of research on POMs, high-resolution imaging techniques based on POMs have proved to be promising methods and have been applied to a variety of imaging modalities, such as photoluminescence (PL) imaging, magnetic resonance imaging (MRI), positron emission tomography (PET), photoacoustic imaging (PAI), computed tomography (CT), ultrasound (US) imaging, and thermal imaging (TI).[64–68]

Among these imaging technologies, magnetic resonance imaging (MRI) has been diffusely used in clinical practice due to its high spatial resolution and non-invasive characteristics; thus, it has become one of the most significant medical imaging techniques for cancer diagnosis.[69–71] However, MRI techniques are less sensitive; thus, contrast agents are often needed to improve image sharpness for small or even molecular information. Contrast agents improve the NMR signal contrast by changing the relaxation process of water particles. NMR contrast agents are mainly divided into T_1 contrast agents and T_2 contrast agents. In terms of the mechanism of action, paramagnetic materials can increase the longitudinal relaxation process (T_1 relaxation process) and make the NMR signal brighter. Superparamagnetic and ferromagnetic materials can accelerate the transverse relaxation process (T_2 relaxation

process) and make the nuclear magnetic signal darker.[72] Due to this property, complexes containing paramagnetic Gd^{3+} and superparamagnetic iron oxide materials are often used as T_1 and T_2 contrast agents, respectively.[73–75] Paramagnetic gadolinium (Gd^{3+}) chelate can be used as an effective MRI contrast agent by shortening the longitudinal relaxation time of water particles, thus enhancing T_1 relaxation and achieving brighter contrast.[76,77] Similar to traditional metal–organic chelates, vacancy POMs, as inorganic ligands and Gd^{3+} to form magnetic clusters, are also expected to accelerate proton relaxation and enhance the MRI signals,[76] which will find a new orientation for the advancement of contrast agents.

With the development of research in recent years, more and more MRI contrast media have been reported. Gd-POMs have been reported as $Gd_2P_2W_{18}O_{62}$ and $K_{15}[(GdO)_3(PW_9O_{34})_2]$, $K_9GdW_{10}O_{36}$ and $K_{11}[Gd(PW_{11}O_{39})_2]$, $K_{15}[Gd(BW_{11}O_{39})_2][Gd(BW_{11})_2]$ and $K_{17}[Gd(CuW_{11}O_{39})_2][Gd(CuW_{11})_2]$, and so on.[78–80] In a recent report, Zong *et al.*[6] integrated GdW_{10} nanoclusters onto the designated $GdW_{10}@Ti_3C_2$ surface of Ti_3C_2MXene nanosheets to construct a multifunctional theranostic nanoplatform. Utilizing the unique capability of POMs in diagnostic imaging and photothermal conversion capability of Ti_3C_2-MXene for tumor hyperthermia, Gd can be used for T_1-weighted magnetic resonance imaging (MRI), while W with high subordinal number ($Z = 74$) can be used for CT. Multimodal imaging can be easily and effectively realized by integrating the nanoparticles with Ti_3C_2MXene. Zong *et al.* evaluated the *in vitro* T_1-weighted MRI performance of $GdW_{10}@Ti_3C_2$ at different concentrations. An obvious concentration-dependent positive enhanced effect was substantial in T_1-weighted MR images (Fig. 5A). Longitudinal relaxation rate r_1 of $GdW_{10}@Ti_3C_2$ was calculated and found to be 7.09 mM^{-1} s^{-1}, which is superior to that of commercial Gd^{3+} chelates ($r_1 = 3.8$ mM^{-1} s^{-1}) (Fig. 5B). Next, to demonstrate the MRI contrast performance *in vivo*, $GdW_{10}@Ti_3C_2$ nanocomposites in PBS were intravenously administered to $4T_1$ tumor-bearing mice, and the T_1-weighted magnetic resonance images were recorded at the time points of 0, 0.5, 1, and 2 h post-injection. The results clearly revealed the gradual accumulation of $GdW_{10}@Ti_3C_2$ in tumor tissues *via* the EPR effect (Fig. 5C), as demonstrated by the continuous enhancement of positive T_1-weighted MRI signals in the tumor. These *in vitro* and *in vivo* results indicated that the as-synthesized $GdW_{10}@Ti_3C_2$ composite nanosheets could serve as a positive-enhancement MRI contrast agent for precise therapeutic guidance and monitoring.

In a study by Davis's group, a stable, high-relaxation MRI contrast agent P_{20}@GdWO was prepared by the self-assembly of the polyoxometrometal $[Gd(W_5O_{18})_2]_9$-(GdWO) with cationic mPEG brush block copolymer containing paramagnetic ions.[17] According to the relaxation stability study of six nanoassemblies with different charge ratios, the nanoassemblies ($^{0.2}P_{20}$@GdWO and $^{0.3}P_{20}$@GdWO) with the ratio of 0.2 and 0.3 have the smallest r_1 variation, respectively, and are the most stable (Fig. 5D). It can also be concluded that the charge ratio has a significant influence on the stability of such POM nanoassemblies combined with cations. Subsequent pH effects and cytotoxicity studies further demonstrated the stability and high

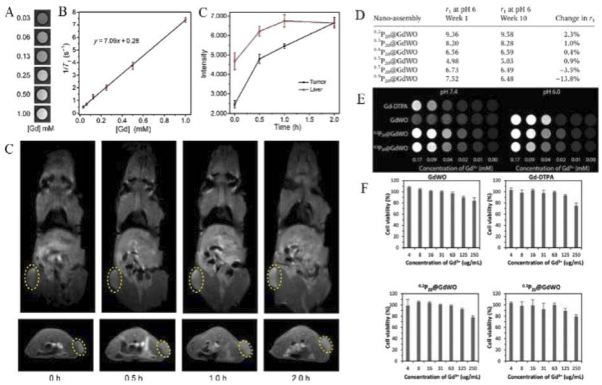

Fig. 5 (A) *In vitro* T_1-weighted MRI and (B) the corresponding T_1 relaxation rate of a GdW10@Ti_3C_2 solution at different Gd^{3+} concentrations ($n = 3$). (C) *In vivo* MRI signal intensity of a tumor and liver of $4T_1$ tumor-bearing mice after i.v. administration of GdW10@Ti_3C_2 at various time intervals (0, 0.5, 1, and 2 h; $n = 3$), and the corresponding T_1-weighted MRI results. Copied with permission.[6] Copyright 2018, with permission from Tsinghua University Press. (D) Relativity measurement of the P_{20}@GdWO nanoassemblies at weeks 1 and 10. (E) T_1-weighted MRI phantom images of Gd-DTPA, GdWO and the selected nanoassemblies $^{0.2}P_{20}$@GdWO and $^{0.3}P_{20}$@GdWO at pH 7.4 and pH 6.0. (F) The low charge ratio nanoassemblies, $^{0.2}P_{20}$@GdWO and $^{0.3}P_{20}$@GdWO, were most biocompatible, showing cell viability just under 80% at the highest tested gadolinium concentration. Copied with permission.[17] Copyright 2018, with permission from RSC Pub.

biocompatibility of $^{0.2}P_{20}$@GdWO and $^{0.3}P_{20}$@GdWO (Fig. 5E and F), which can be potential candidates for contrast agents.

Polymer-based carriers have the advantages of good biocompatibility, stimulus responsiveness, and modifiability. Organically modified POMs can achieve better biocompatibility and improve the r_1 value of high-sensitivity MRI.[81,82] Wu *et al.*[83] encapsulated Gd-POMs with an amphiphilic molecule containing poly(ethylene oxide) (PEO) and quaternary ammonium group to form water-soluble organic–inorganic hybrid molecules, which could further self-assemble into regular vesicle structures. The results show that the vesicle aggregates can effectively accelerate the relaxation of water particles, and further improve the intensity of MRI contrast. This provides an experience for subsequent studies that proton relaxation can be accelerated and MRI performance can be improved by introducing hydrophilic groups. These Gd-POM MRI findings further improve the level of accurate diagnosis of cancer and lay a good foundation for subsequent treatment.

Moreover, the development of multiple functional materials combining MRI/CT imaging with cancer therapy will facilitate clinical diagnosis and treatment. Zhang *et al.*[84] assembled a novel food-borne antioxidant peptide (Lys-Asp-His-Cys-His-Val-Thr-Pro-Tyr) extracted from sea trepang protein hydrolysate with high radical-scavenging ability with POMs to obtain supramolecular complexes with MRI and CT imaging functions, along with photothermal characteristics. The developed K–Gd has good biocompatibility and stability, and can maintain a good uniform particle size (3–4 nm) under physiological conditions. It was shown that K–Gd has good MRI and CT properties, and exhibits excellent photothermal properties by

reduced K–Gd (rK–Gd). This shows that K–Gd has good comprehensive diagnostic and therapeutic ability. These findings of Gd-POM MRI contrast agents have further improved the level of accurate diagnosis of cancer and laid a good foundation for subsequent treatment.

2.4 Photothermal therapy

Photothermal therapy (PTT) is an emerging cancer treatment based on the principle of photothermal conversion.[85–87] The tissue penetration of near-infrared light is stronger than that of visible and ultraviolet light, and it shows lesser damage to normal tissues. PTT can effectively convert the absorbed near-infrared (NIR) light energy into local hyperthermia, which causes DNA damage, cell membrane destruction, and protein denaturation of cancer cells, ultimately leading to cell death.[88] This highly effective and mild treatment modality has attracted much attention.

An ideal photothermal dose should exhibit good biocompatibility and strong absorption in the near-infrared region and can be effective in converting the absorbed near-infrared light energy into thermal energy. In recent years, great research progress has been made in the corresponding nanomaterials for PTT, such as carbon nanomaterials,[89] gold nanostructures,[90] palladium nanosheets,[91] and organic nanomaterials, such as near-infrared absorption conjugated polymers[92,93] and nanomicelles-encapsulated NIR dyes.[94]

In recent years, NIR photothermal therapy based on reduced POMs has been developed. In this regard, Shi's team reported a molybdenum (Mo)-based polyoxometalate (POM) cluster as an ideal near-infrared (NIR) photothermal agent whose diameter is small (about 1 nm) in size in blood circulation and then self-assembled into tens of nanometers in tumors triggered by the TME.[13] Because these POM clusters have the property of low pH-induced self-assembly, a suitable acidic environment in tumor cells facilitates POM clusters to bind to protons (Fig. 6A). After binding, the surface charge of POM clusters decreases and the electrostatic repulsion between each other decreases, which in turn promotes the occurrence of self-assembly. The resulting nanoparticles can enhance the EPR effect, and moreover, the selective retention in the tumor is more significant, which allows POMs to produce passive targeting. At the same time, the production of self-assembly also enhances the reducing ability of Mo and enhances the migration of near-infrared absorption and absorption peaks. It is found that the NIR absorption is significantly blue-shifted to 808 nm, which is one of the NIR lasers with high penetration depth applied in clinical practice. Also, a wide range of adjustable photothermal conversion at 808 nm resulted in a more effective temperature rise. The pharmacokinetics study of POMs revealed that most of them can be excreted within a week after injection into the body (Fig. 6B), thanks to their very small hydrodynamic diameter of 1.7 nm and excellent hydrophilicity in neutral medium. This property, which allows rapid excretion and clearance, can avoid potential long-term toxicity *in vivo*. More importantly, in POM-mediated photothermal therapy, the temperature of the tumor reached above 47 °C under whole area irradiation, while the temperature of nearby normal tissues remained below 42 °C (Fig. 6C). This increase in the temperature contrast allows effective tumor suppression without damage to non-tumor areas and is highly selective for tumors. All these results confirm that POMs are intelligent *in vivo* acidic and reductive photothermal agents, whose therapeutic efficiency can be enhanced by adaptive absorption changes and self-assembly aggregation in the tumor microenvironment.

In another scheme, a highly negatively charged mega-rota-like POM ($Na_{15}[Mo^{VI}_{126}Mo^{V}_{28}O_{462}H_{14}(H_2O)_{70}]$, Mo_{154}) is encapsulated by an organic dendrimer (D-3) with a cationic head and a triethylene glycol (TEG) chain tail (Fig. 7).[11] This hybrid formed by external encapsulation design has unique advantages: (1) increases the biocompatibility of POMs and avoids the cytotoxicity caused by the binding of exposed POMs to biomolecules such as proteins; (2) dendrimers bring sufficient drug molecule loading space; and (3) can be controlled by thermal response. POMs fully encapsulated by cationic dendrimers can form uniform micellar particles with particle size less than 10 nm under physiological conditions. Moreover, the micelles have excellent photothermal properties. Due to their

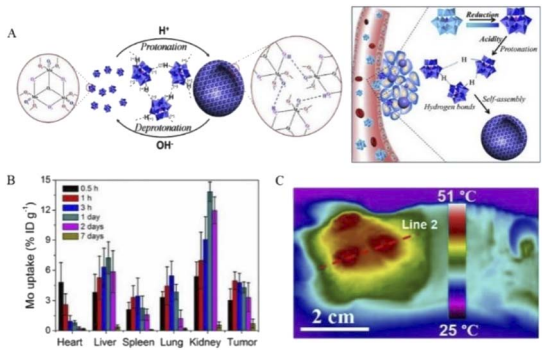

Fig. 6 (A) Schematic representation of protonation-induced self-assembly of POMs units into hollow aggregates with adaptive behavior in response to intratumoral acidity and reducibility. (B) Distribution of Mo in $4T_1$ tumor-bearing mice over 0.5 h to 7 days. (C) Representative thermal image of 808 nm laser irradiation.[13] Copyright 2016, with permission from American Chemical Society.

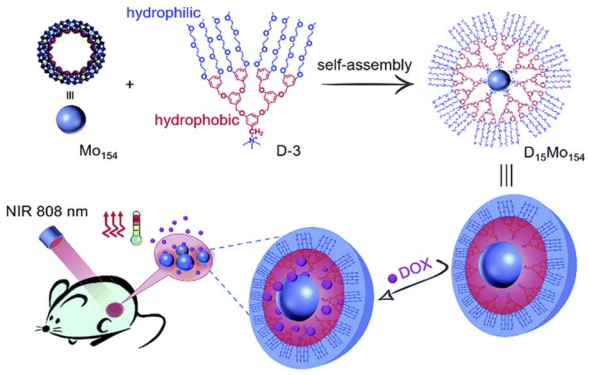

Fig. 7 Structural illustration of $D_{15}Mo_{154}$ micelles platform preparation and multifunctional carrier and laser irradiation drug release.[11] Copyright 2018, with permission from Royal Society of Chemistry.

thermal response effect, in the presence of loaded DOX, the temperature of the complex increases and the drug can be rapidly released by near-infrared irradiation. Such micelles form a composite platform that can be used both for photothermal therapy of tumor tissue and as drug carriers to control the release of drugs.

2.5 Enzyme inhibitors

POMs, as a drug used in the treatment of cancer, have been used to prepare many different derivatives, among which POMs have also been found to affect the activity of some enzymes, such as alkaline phosphatase, caspases, and histone deacetylase (HDACs). The inhibition or activation of these enzymes can make cells undergo apoptosis, and then make the tumors fade, thus achieving the purpose of anticancer.

2.5.1 Alkaline phosphatase inhibitor. Alkaline phosphatases (APs) are highly expressed in osteoblasts during active bone growth and are mineralized by the hydrolysis of inorganic pyrophosphate for bone growth. When the cells in the bone become cancerous or the cancer cells spread to the bone, the invasion of the bone will increase and the bone turnover will increase, eventually leading to bone formation disorder, and the patient's Aps will be overexpressed.[95,96] Therefore, elevated Aps levels are considered as a nonspecific tumor marker and an important target in the field of anticancer drug development.

Jamshed *et al.*[5] synthesized seven polytungstate compounds and investigated the inhibition of two isoenzymes of alkaline phosphatase (non-specific (TNAP) and tissue-specific (IAP) alkaline phosphatase). $Na_{10}[H_2W_{12}O_{42}]\cdot 27H_2O$ (A6) had the highest inhibitory effect on IAP with a K_i value of 313 ± 7 nM, while compound $Na_{33}[H_7P_8W_{48}O_{184}]\cdot 92H_2O$ (A3) had the highest inhibitory effect on TNAP with a K_i value of 313 ± 7 nM. The maximum inhibitory effect of A3 on TNAP can be due to its flexible polyhedral structure, which provides optimal spatial location for interaction with TNAP. Levamisole is a commonly used normal inhibitor of TNAP, and its inhibitory effect is in the micromole range, while the potency of the reported inhibitors is several times that of the standard inhibitors. L-phenylalanine is a common normal inhibitor of IAP with a 78% inhibition rate at 5 mM, while all reported compounds showed activity of over 70% when tested at a concentration of 0.1 mM, with A6 showing the highest activity. The result shows that the new polytungstate has strong inhibition on Aps.

As a drug, while killing cancer cells, it is necessary to ensure that it does not kill normal cells and is safe. Using vincristine as a standard inhibitor, the effects of the compound on the growth and proliferation of H157 cancer cells and normal HCEC cell lines were examined by the MTT assay. The results showed that all POMs had little influence on HCEC, but had good cytotoxicity against H157 in a dose-dependent manner. $Na_{16}[(O_3POPO_3)_4W_{12}O_{36}]\cdot 38H_2O$ (A4) showed the highest antiproliferative activity against H157, and its cytotoxicity was approximately 65% at a terminal concentration of 100 nM. The remaining compounds also showed significant cytotoxicity when examined at various concentrations (100 nM to 100 μM) (Fig. 8). Moreover, reducing the compound concentration had little influence on its antiproliferative activity, even at the 100 nM terminal concentration, the antiproliferative activity of all compounds remained around 60%, with the exception of A1 and A2, showing 38% and 56% activity, respectively, at the 100 nM terminal concentration. In comparison with vincristine, its activity was 47% at a final concentration of 100 μM. These polytungstic compounds showed a much stronger inhibitory effect than the standard inhibitor vincristine. This powerful anticancer activity makes its use in cancer therapy very promising.

The cytotoxicity studies of these compounds on cancer cells and human corneal epithelial undead cells revealed that these compounds had only low cytotoxicity against normal human cell lines, indicating that these compounds may be a good choice for the treatment of cancer. At the same time, all anticancer drugs can cause immune system damage, and patients are vulnerable to exogenous infection when their immune function is low due to the influence of drugs. In particular, infections caused by *Acanthamoeba* cause granulomatous amoeba encephalitis (GAE), which has a high fatality rate. Synthetic polytungstate is also reported to have a potent lethal effect on *Acanthamoeba*. Therefore, the report of polytungstate provides us with a novel approach for cancer treatment, namely, the simultaneous control of elevated alkaline phosphatase levels and granulomatous amoebic encephalitis. In this way, the death caused by infection caused by external causes can be well reduced and the survival rate of cancer patients can be greatly improved.

2.5.2 Activation of caspases. Apoptosis, also known as programmed cell death, is controlled by pro-apoptotic caspases.[97,98] The apoptotic cascade amplification reactions of caspases are initiated *via* the following two major pathways—a mitochondrial pathway (the release of cytochrome C from the mitochondria) and the death receptor pathway (the activation of death receptors in response to ligand binding).[99] After these two pathways are triggered, caspases that determine apoptosis are activated, leading to cellular protein degradation, which in turn leads to apoptosis. Also, most of the effects of chemotherapeutic drugs on cancer cells belong to the mitochondrial

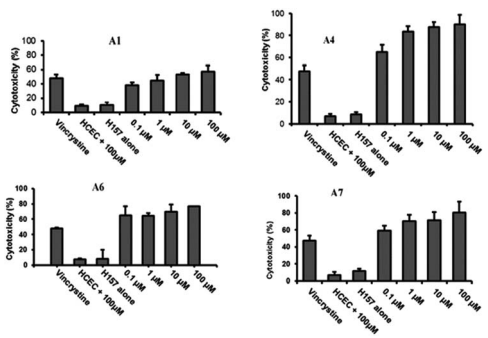

Fig. 8 There is a significant difference in the effect of POMs on H157 and HCEC. A1, A4, A6, and A7 showed significant cytotoxicity toward H157 and HCEC. Vincristine as a positive control, concentration 100 μM. Copied with permission.[5] Copyright 2012, with permission from Royal Society of Chemistry.

apoptotic pathway.[100] Among the caspase family, caspase-3 is a key enzyme in the process of stimulation-induced apoptosis.[101,102] Once activated, caspase-3 is free to participate in various processes of apoptosis.

Wang *et al.*[12] synthesized a novel cobalt-based polyoxometalate $(Himi)_2[Bi_2W_{20}O_{66}(OH)_4Co_2(H_2O)_6Na_4(H_2O)_{14}]\cdot 17H_2O$ (imi = iminazole) (BWCN) (Fig. 9A). In the report, BWCN can significantly inhibit the proliferation of cancer cells, and as a chemotherapeutic drug can also induce the apoptosis of HT-29 cancer cells by induction, and show significant cleaved-caspase-3 expression. HT-29 cells were treated with 160 μmol L^{-1} BWCN for 24 h and then observed for changes in cell morphology under an inverted microscope. HT-29 cells showed shrinkage, rounding, and fragmentation after treatment compared with the control cells (Fig. 9B). HT-29 cells were treated with 160 μmol L^{-1} BWCN for 24 h and stained with Hoechst 33342. It was found that HT-29 cells underwent typical apoptotic morphological changes, including apoptotic body formation, nuclear fragmentation, and chromatin condensation (Fig. 9C). Meanwhile, HT-29 colon cancer cells treated with BWCN for 24 h were detected by Western blotting, and cleaved caspase-3 expression (17 kd and 20 kd) was detected (Fig. 9D). The results showed that cleaved caspase-3 expression was upregulated after treatment with BWCN. A comparison of the experimental data showed that BWCN finally induced HT-29 cell apoptosis by activating caspase-3. It indicates that BWCN has significant inhibitory effect on cancer cells and has great potential for cancer treatment.

Li *et al.*[8] developed an arsenopolybdate $(K_2Na[AsMo_6O_{21}(-O_2CCH_2NH_3)_3]\cdot 6H_2O)$, evaluated it by human leukemia cells (HL-60 and U937), and showed antileukemia activity. The nuclear morphology analysis showed that with the increase in the compound dose, the nucleus decreased and the number of dead cells increased. When the concentration was 10 μM, a large number of apoptotic cells began to appear. Thus, this compound could induce apoptosis in HL-60 and U937 cells in a dose-dependent manner.

Flow cytometry was next used to further confirm the effect of the compounds on apoptosis in HL60 and U937 cells. After the cells were treated with compounds for 24 h, the cells were double stained with annexin V/PI. In the results shown in Fig. 10A, the upper left corner shows mechanically damaged cells, the lower left corner shows normal viable cells, the upper right corner shows late apoptotic and necrotic cells, and the lower right corner shows early apoptotic cells. The apoptotic rate in Fig. 10B showed that the apoptosis rate of HL-60 cells treated with 8 μM compound increased from 4.73% in the control group to 43.40%. However, in U937 cells treated with 14 μM compound, the apoptosis rate increased from 7.27% in the control group to 67.00%. The addition of the compound significantly increased the apoptosis of cells. The activation of caspase-3 plays a very important role in the apoptosis pathway; however, bcl-2 can inhibit apoptosis.[103] In Fig. 10C and D, the expression of active caspase-3 of HL-60 and U937 was significantly increased by 104–126% and 101–120%, respectively. The expression of Bcl-2 in HL-60 and U937 was significantly decreased by 109–115% and 115–215%, respectively, which was consistent with the change in the apoptosis rate. This also demonstrates that apoptosis can be induced in leukemia cells by activating caspase-3 expression and downregulating Bcl-2. This POM compound can therefore be a potential candidate for the treatment of acute promyelocytic leukemia in the future.

2.5.3 Histone deacetylase inhibitor. Histone deacetylases (HDACs) can mediate changes in nucleosome conformation and play an important role in the regulation of gene expression.[104,105] HDACs can be involved in cell cycle progression and differentiation, and their relaxation has been implicated in a variety of cancers.[106,107]

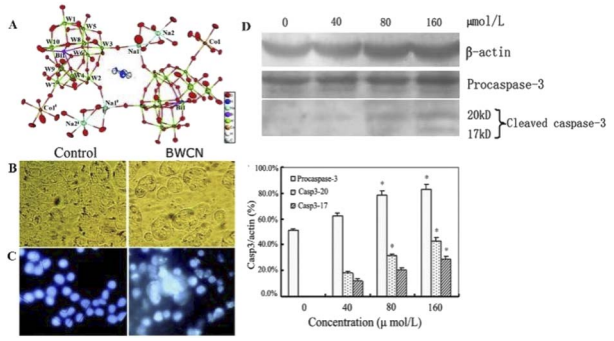

Fig. 9 (A) The crystal structure diagram of BWCN. (B) HT-29 cells began to shrink, round, and fragmented compared with untreated cells (photographed by inverted light microscope, 200×). (C) HT-29 cells treated with 160 μmol L^{-1} of BWCN for 24 h were stained with Hoechst 33342 (observed under a fluorescence microscope, 200×). (D) The expression of caspase-3 and β-actin in the HT-29 cells treated with different concentrations of BWCN for 24 h. The cell lysates were separated on a 10% SDS-PAGE gel, transferred to a nitrocellulose membrane, and probed with *anti*-β-actin, or anti-cleaved-caspase-3 antibodies. The protein content was normalized byβ-actin. *$p < 0.05$, compared to the control group.[12] Copyright 2014, with permission from Royal Society of Chemistry.

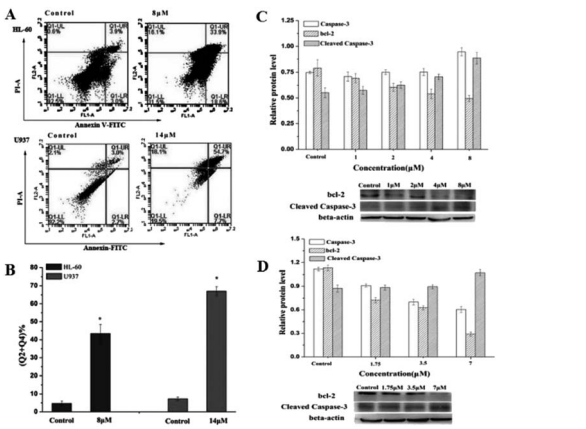

Fig. 10 Flow cytometry was used to detect apoptosis in HL-60 cells treated with 8 μM compound and U937 cells treated with 14 μM compound for 24 h. Copied with permission; The compound regulated the expression of apoptosis-related proteins in HL-60 cells (C) and U937 cells (D) and statistical results. Copied with permission.[8] Copyright 2017, with permission from Elsevier.

In cancer cells, HDAC is overexpressed, which leads to enhanced deacetylation, restoring the positive charge of histones, increasing the attraction between DNA and histones, and making the relaxed nucleosomes very tight. This makes some tumor suppressor genes unable to be smoothly expressed, which leads to cancer cells that are not prone to apoptosis.[106] Histone deacetylase inhibitors (HDACI), by inhibiting HDAC activity, enhance histone acetylation in specific regions of chromatin and restore the expression of many tumor suppressor genes, thereby regulating the expression and stability of apoptosis and differentiation-related proteins. It can induce apoptosis and differentiation of cells, and become a new class of antitumor drugs. For example, trichostatin A (TSA) and suberoyllaniide hydroxamic acid (SAHA) have been shown to have antitumor effects.[108] HDACI not only has a good therapeutic effect on a variety of hematological tumors and solid tumors, but also has the advantages of relatively high selectivity and low toxicity of tumor cells.

Dong *et al.*[7] obtained five POM compounds with HDAC inhibitory activity by screening from a polyoxometalate library (Fig. 11). One of the new tri-organic-tin-substitute germanotungstate $K_3H[\{(n\text{-Bu})Sn(OH)\}_3GeW_9O_{34}]\cdot 26H_2O$ (PAC-320) exhibited outstanding HDAC inhibitory activity. Compared with several others, PAC-320 has excellent anticancer effects *in vivo* and *in vitro*.

The effect of PAC-320 on intracellular acetylated histone H3 levels was determined by immunoblotting, and then its inhibitory activity against HDAC in cancer cells was verified. H22 mouse hepatoma cells were treated with different doses of PAC-320, and total proteins were extracted and analyzed by sodium dodecyl sulfate polyacrylamide gel electrophoresis (SDS-PAGE) and immunoblotting with acetylated H3-specific antibodies. Analysis revealed that the H3 acetylation level of the H22 cell line was low, and PAC-320-induced histone H3 hyperacetylation occurred in a dose-dependent manner. This shows that PAC-320 has a significant effect on both the histone acetylation of nucleosomes *in vivo* and on theHDAC activity *in vitro*, which verified that these compounds effectively inhibited HDAC activity *in vitro* and *in vivo*.

To examine the effects of PAC-320 on the growth and proliferation of a variety of tumor cells, researchers used the MTT assay and found that PAC-320 inhibited the growth of not only mouse hepatoma cells (H22) but also a variety of human cancer cells, including colon cancer cells (SW620), gastric adenocarcinoma cells (MGC-803), lung cancer cells (A549), breast cancer cells (MM-231), and hepatoma cells (HepG2), which showed some dose-dependent characteristics. In addition, the results showed that PAC-320 was effective against a variety of cancer cells, with IC_{50} values at the micromolar level. All these clearly indicate that PAC-320 has strong antitumor cell proliferation effect *in vitro*. Meanwhile, the toxicity of PAC-320 toward normal cells was investigated using the MTT assay. The results showed that PAC-320 small hepatocellular carcinoma cells HepG2 had significant antiproliferative effect, but had less toxicity toward normal hepatocytes L-02. Moreover, its IC_{50} value in cancer cells was much lower than that in normal cells, which also indicated that PAC-320 had better safety.

In order to further evaluate the anticancer effect of PAC-320 *in vivo*, animal simulation experiments were performed using the H22 hepatocellular carcinoma mouse model. The results showed that on day 14, tumor growth was inhibited by 62.5% and the tumor weight was significantly reduced in PAC-320 (300 mg kg^{-1})-treated mice compared to the control mice treated with only thinner (normal saline). At the same time, the growth of the mice was not found to be inhibited. In contrast, tumor growth was reduced by 95.5% on day 14 after cyclophosphamide (CTX). However, the growth of mice was also inhibited by CTX, which indicates that it has side effects on the normal growth and development of mice. This shows that PAC-320 has significant antitumor activity *in vivo* and has little effect on the normal growth and development of animals. These data indicate that PAC-320 has significant HDAC inhibitory activity in cells, and has anticancer ability *in vitro* and *in vivo*, with almost no damage to normal growth of cells and animals. PAC-320 could be a promising anticancer drug.

Based on the above discussion, POMs control the life activities of cancer cells by regulating related enzymes and causes the apoptosis of cancer cells by inhibiting or activating enzyme activities. This method opens up a new strategy for POMs in cancer treatment. In the future, multiple POMs can be used together to build a multi-target drug platform, or combined with traditional drugs to play a synergistic role and improve the effectiveness of existing anticancer drugs. Through the further study of enzymes, the application of polyoxometalates in this direction will have a great prospect.

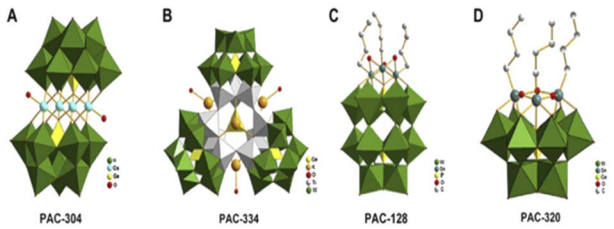

Fig. 11 (A) $[Co_4(H_2O)_2(GeW_9O_{34})_2]^{12-}$ (PAC-304); (B) $[(GeO_3)(OH)(GeW_9Ti_3O_{38})_3]^{22-}$ (PAC-334); (C) $[(BuSn)_3P_2W_{15}O_{59}]^{9-}$ (PAC-128); (D) $[\{(n\text{-Bu})Sn(OH)\}_3GeW_9O_{34}]^{4-}$ (PAC-320).[7] Copyright 2011, with permission from Elsevier.

3. Antibacterial application of polyoxometalates

Bacterial infections, one of the most challenging problems in medicine, threaten the lives of millions of people worldwide due to the emergence and rapid spread of bacterial resistance to existing antibiotics, as well as limited progress in the discovery and development of new and effective antibacterial drugs. At present, drug-resistant infections may lead to new problems, such as longer hospital stays, higher admission rates, higher drug costs, more difficult post-discharge care, and higher mortality.[109] In the study of emerging infectious diseases in the world, it is found that more than half of the pathogens of

emerging infectious diseases are drug-resistant bacteria, which fully shows that drug-resistant bacteria have appeared widely. In addition to the serious damage to public health, this emerging strain of drug-resistant bacteria could also pose a significant burden on the global economy.[110]

The traditional way of treatment of infectious diseases is the use of antibiotics, such as ciprofloxacin, doxycycline, and cephalosporin. These traditional antibiotics can be applied to specific biological molecular targets by preventing cell DNA replication and repair, protein synthesis, and cell wall turning process to selectively inhibit or kill the microbial cells.[111] However, years of overuse, and even abuse, have made pathogenic bacteria resistant to almost all conventional antibiotics available, either by mutating or acquiring resistant genes from other organisms. This makes antibiotic resistance of microorganisms ineffective in the treatment of infectious diseases an urgent problem to be solved.[112]

Currently, the commonly used method to overcome antibiotic resistance is the combination of multiple antibiotics. However, the effectiveness of this regimen has some limitations because it requires the accurate analysis of the patient's pathogens to achieve the best efficacy, and because of the potential antagonism and unknown side effects between different antibiotics, it is not always successful in achieving therapeutic effects. Therefore, new effective antibacterial drugs are urgently needed to alleviate or reverse the crisis caused by bacterial resistance. Table 2 summarizes the antibacterial studies of POM-nanocomposites in the past two years. It can be seen that POMs have great application potential in antibacterial aspects.

3.1 Hybrid nanocomposites

Hybrid nanocomposites have great research value in pharmacology and medicine because drug delivery systems based on nanocomposites are very promising for targeted therapies that can deliver therapeutic agents with improved properties to their destination while minimizing side effects.[113,114] Because the composition of nanocomposites is often very different in their structure as well as physical and chemical properties, their combinations and synergies offer a great deal of possibilities in terms of function and biological activity.[115] POMs have proven to be ideal building blocks for nanocomposites due to their unique range of properties and ability to form clusters ranging in size from a few angstroms to nanometers. In addition, embedding POMs into nanocomposites can not only increase the diversity of composites but also reduce the toxicity of POMs, achieving a win–win effect.

3.1.1 POM-peptide nanocomposites. According to previous studies, compounds containing peptides have good pharmacological activities, such as antibacterial activity.[116] Therefore, it would be a good strategy to enhance the antimicrobial properties of POMs by modifying them using peptides.

Zhang *et al.*[4] reported a novel composite (AgPW@PDA@Nisin) consisting of surface-conjugated nisin (an antibacterial 34 amino acid polycyclic peptide) on the surface of polydopamine (PDA) as a shell and polyoxometalate ($Ag_3PW_{12}O_{40}$ = AgPW) as a core to form lactin with a putamen structure (Fig. 12). This AgPW@PDA@Nisin has potential antibacterial activity against *S. aureus*. The minimum inhibitory concentration (MIC) and minimum bactericidal concentration (MBC) of the composite were 4 μg mL^{-1} and 32 μg mL^{-1}, respectively, and the antibacterial effect of the composite was better than that of the single component. The cytotoxicity of human dermal fibroblasts toward HDF-a (human dermal fibroblasts) cells was measured by the MTT assay. The cytotoxic concentration of the complex was very low, and the cell survival rate was nearly 100% at a high concentration of 128 μg mL^{-1} at 24 h. Therefore, the fungicide AgPW@PDA@Nisin has a high safety *in vitro*.

Table 2 Overview of the antibacterial application of POM-nanocomposites[a]

POM-type	Antibacterial activity	Ref.	POM-type	Antibacterial active on	Ref.
CTAB/POMs@hydrogel matrix	*E. coli* *S. aureus*	117	AgNPs/INH@PTA and AgNPs/INH@PMA	*E. coli* *S. aureus*	118
Antioxidant peptide-GdW_{10}*	*E. coli*	84	QACs-$[(BuSn)_3(\alpha\text{-}SiW_9O_{37})]$	*E. coli*	119
CS/SiW-PAM hydrogel	*E. coli*	120	SHCMN-rPOMs*	*E. coli*	121
AgPW@PDA@Nisin	*S. aureus*	122	$(NR_4^+Cl^-)$/POMs and Ormosil/POMs	*CR P. aeruginosa* *E. coli* *MR S. aureus* *B. subtilis*	123
AIPH/POM/PEGDA*	*MR S. aureus*	124	PEG-grafted chitosan@POMs	*E. coli* *S. aureus*	125
CF-POMs	*E. coli* *S. aureus* *B. subtilis*	126	$[AgP_5W_{30}O_{110}]^{14-}$ (AgP_5W_{30})	*E. coli* *MR S. aureus* *S. aureus*	127
Fe_3O_4@PDA@Ni-DT	*AR/KR E. coli*	128	$[\{(p\text{-tolyl})SbIII\}4(A\text{-}\alpha\text{-}XW_9O_{34})_2]^{n-}$	*E. coli* *B. subtilis* *V. parahaemolyticus* *V. vulnificus*	129

[a] CTAB: hexadecyl trimethyl ammonium bromide; *: photothermal/thermodynamic therapy; CS: chitosan; PAM: poly(acrylamide); PDA: polydopamine; AIPH: 2,2′-azobis[2-(2-imidazolin-2-yl)propane]dihydrochloride; PEGDA: poly(ethylene glycol) diacrylate; CF: ciprofloxacin; MR: methicillin-resistant; AR: ampicillin-resistant KR: kanamycin-resistant; CR: ciprofloxacin-resistant; Ni-DT: $[Ni(HL)_2]_2[W_{10}O_{32}]\cdot 4H_2O$, HL: 2-acetylpyridine thiosemicarbazone; INH: isonicotinylhydrazide; SHCMN: soybean pentapeptide Ser-His-Cys-Met-Asn.

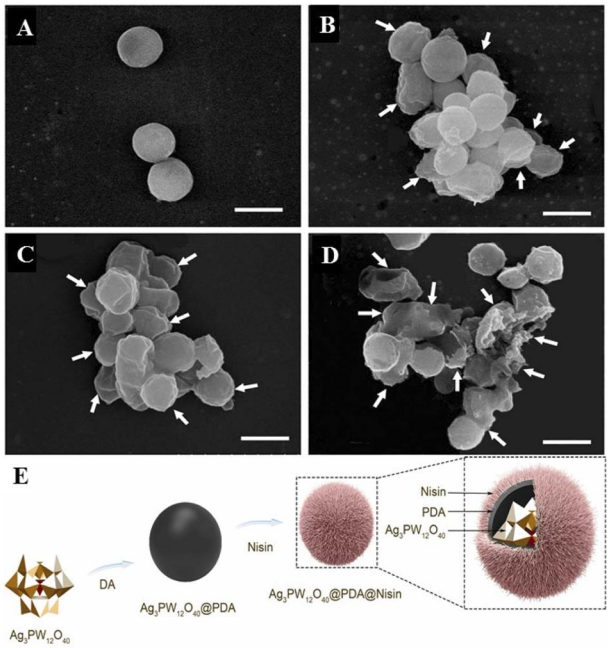

Fig. 12 The effect of AgPW@PDA@Nisin on the morphological changes of *S. aureus*. Cells were treated with 4 μg mL^{-1} AgPW@PDA@Nisin for (A) 0 h, (B) 6 h, (C) 12 h, and (D) 24 h. White arrows indicate wrinkled and ruptured membrane structures; (E) AgPW@PDA@Nisin's composition diagram.[4] Copyright 2020, with permission from Elsevier.

The detection of intracellular components in the supernatant is a good indicator of membrane integrity. The UV absorption of the cell supernatant was found to increase rapidly in the first hour by detecting the absorbance at 260 nm. Thereafter, the values changed more slowly than in the first hour, and after 3 h, the values reached a steady state. This shows that the intracellular nucleotides leak out. The content change curve of nucleotides showed that the degree of bacterial membrane damage was directly proportional to dose and time. This shows that the composite can destroy the cell membrane of *S. aureus* and release its intracellular components. Normally, β-galactosidase in the cytoplasm leaks to the outside of the bacteria and is detected at 420 nm only when the cell membrane is damaged. By detection, it was found that at 420 nm, the absorbance values continued to increase within 6 h after treatment with different concentrations of nisin nanoflower drugs. The results showed that AgPW@PDA@Nisin increased the membrane permeability of *S. aureus*, resulting in the leakage of key enzymes into the supernatant. Meanwhile, as observed by SEM, after 6 h of complex treatment (Fig. 12A–D), the cells became wrinkled and depressed. After 12 h, the cells became shriveled, depressed, irregular, and adhered to each other, which may lead to the exudation of the cytoplasm within the bacteria. After 24 h, most cells were broken. It can be concluded that AgPW@PDA@Nisin can cause serious damage to the plasma membrane of the cell, resulting in the outflow of intracellular substances, leading to bacterial apoptosis, thus exhibiting antibacterial ability.

3.1.2 POM-modified magnetic nanocomposite. Magnetic microparticles (MMPs) have received increasing attention due to their high magnetic saturation and good dispersion. In particular, superparamagnetism makes them easy to collect and redisperse under the intervention of an external magnetic field.[130–132] For example, magnetite (Fe_3O_4) and its series of composites, Fe_3O_4@PDA,[131,133] AgNPs-Fe_3O_4@PDA,[134] and Au@PDM/Fe_3O_4,[135] are ideal candidates for biological applications as labels for magnetic resonance imaging or active agents for antitumor therapy, or even as biocatalytic materials. In addition, due to the high magnetic responsiveness of Fe_3O_4 nanoparticles, the material is easily separated from the suspension in a magnetic field and is easy to reuse, which greatly reduces the cost. Dopamine (DA), a naturally-occurring neurotransmitter in living organisms, has many valuable characteristics. For example, when oxidized and self-polymerized in alkaline conditions, it shows strong adhesion to almost any material surface, which means that it can be used as a multipurpose intermediate layer to modify different substrates or other nanostructures to provide or enhance specific functions.[136,137] In addition, the structure of PDA has many functional groups, such as quinine, amine, and imine, which are good coordination sites for connecting metal ions or metal–ligand complexes, and polymer-inorganic core/shell structures with adjustable functions can be produced by attaching to these sites.[138]

Fang *et al.*[2] reported a polyoxometalate-modified magnetic nanocomposite Fe_3O_4@PDA@POM. The composite was prepared by coating $[Cu(HL)_4]_2[P_2Mo_5O_{23}]_2 \cdot 8H_2O$ (POM, L = 2-aminopyridine) on preassembled polydopamine (PDA)-modified carboxyl-functionalized Fe_3O_4 magnetic microspheres. Then, the composite material was used to treat *Escherichia coli* and *Streptococcus albicans*, and the antibacterial potential of the material was qualitatively and quantitatively evaluated by the colony counting method, as shown in Fig. 13 ($n = 4$). The comparison between the single molecule and the composite material shows that the antibacterial performance of the Fe_3O_4@PDA@POM nanocomposite is significantly better than that of Fe_3O_4 and Fe_3O_4@PDA, and

Fig. 13 Photograph of (A) *E. coli* and (B) *S. albumin* colonies on plates (16 h after culture).[2] Copyright 2019, with permission from Royal Society of Chemistry.

the POM-functionalized material shows a higher effect than that of the single PDA-doped material.

In order to further explore the potential of POMs, POMs, L, Cu^{2+}, and $[P_2Mo_5O_{23}]^{6-}$ polyoxyanion were introduced into the experimental system. The results showed that Cu^{2+} had high antibacterial activity against *E. coli*, confirming that Cu^{2+} in POMs may be the most effective part to improve the antibacterial performance. The composites reported at the same time were recyclable; the Fe_3O_4@PDA@POM nanocomposites were cleaned with ethanol and water, and then reused in the next cycle. Even after six cycles, its antibacterial performance was up to 90%. It shows that the material has good repeatability. Therefore, the Fe_3O_4@PDA@POM nanocomposite has high recyclability and simplified separation process, which is expected to enrich the practical application of POMs in antibacterial materials research. The stability test results confirmed that the prepared Fe_3O_4@PDA@POM nanocomposites maintained high stability for 12 h in solution (pH value of 6–8, 0.75% NaCl solution and physiological buffer of water).

Several possible bactericidal mechanisms of Fe_3O_4@PDA@POM nanocomposites were also studied in this paper: (1) a large area of cationic surface Fe_3O_4@PDA@POMs can act as a "nanohunter", giving it easy access to negatively charged bacterial cell walls and, in this way, causing electrostatic damage to cell membranes, resulting in the leakage of the intracellular material. (2) As POMs are water-soluble, while POMs on nanocomposite materials exist on the surface of the polymer, POMs on nanocomposite materials can be partially dissolved in water with the extension of the experiment time. POM targets include related enzymes/proteins on cell membranes and certain REDOX reactions, such as respiration or other redox processes.[139] Due to their high redox activity, POMs can interfere with bacterial respiratory system by oxidizing some important electron carriers, thus affecting the production of ATP.[140] In the reported experiments, POMs have been shown to affect respiratory chain dehydrogenase activity, which in turn causes fatal damage to bacterial cells. (3) POMs can increase the ROS levels by directly oxidizing proteins, lipids, and other bacterial substances. Glutathione (GSH) is a tripeptide containing sulfhydryl groups that acts as an antioxidant for bacteria, preventing cellular component damage caused by oxidative stress.[141] POMs can increase the ROS levels by oxidizing GSH, resulting in GSH depletion.[142] (4) Another potential mechanism is that once the cell walls are destroyed, because of the electrostatic properties of POMs, cytoplasm, and positively charged areas or protein interactions, L can also enhance the amine in the nanocomposites and the electrostatic force between the bacterial cell membrane, and the release of the copper ions can lead to the instability of the cell wall or damage, interfering with the respiratory chain.[143]

In general, the leakage of nucleic acids and proteins, disruption of respiratory chain dehydrogenase activity, accumulation of ROS, and loss of GSH are all factors leading to bacterial cell death. The antibacterial effect of Fe_3O_4@PDA@POM nanocomposites is achieved by multiple interactions of multiple components, and the combined effect of these interferences eventually leads to bacterial cell death.

3.2 Synergistic antibacterial activity

It is also a good strategy to help conventional antibiotics work by regulating cells with polyoxometalates. Hyperpolarization, in biology, is a change in the cell. During this time, the charge distribution of the cell changes (Fig. 14A), which are related to the outflow of cations and inflow of anions within the cell, thereby reducing the negative charge within the cell.[3] For example, *Bacillus subtilis* can prevent hyperpolarization by increasing Mg^{2+} influx, thus regulating ion flux to resist antibiotic effects.[3] Therefore, it is important to find ions or NPs that can strongly interact with cell membranes and interfere with the cationic influx process for the treatment of multidrug-resistant bacterial infections. Polyoxometalates (POMs) have been developed because of their highly charged ions. Due to its high surface charge density and abundance of oxygen and hydrogen oxygen ligands, POMs can selectively bind to certain protein surfaces.[14] It can also be strongly adsorbed onto the lipid membrane and induce phase and morphology instability of the lipid membrane. It is of great significance to disintegrate the stability of bacterial cells and induce cell death. Preyssler-type POMs has ultra-small size, good thermal and hydrolytic stability, and a well-defined surface structure with a high affinity for biological macromolecules.[144]

Chen *et al.*[14] reported that two Preyssler-type polyoxometalates ($[NaP_5W_{30}O_{110}]^{14-}$ or $[AgP_5W_{30}O_{110}]^{14-}$) were co-antibacterial with antibiotic combinations, having high antimicrobial efficiency and low risk of resistance. Here, we measure the cell hyperpolarization using a fluorescent membrane potentiometer dye thioflavin-T (ThT).[145] This is because ThT is a positively charged organic dye and since the inner membrane of the cell is negatively charged, it can remain

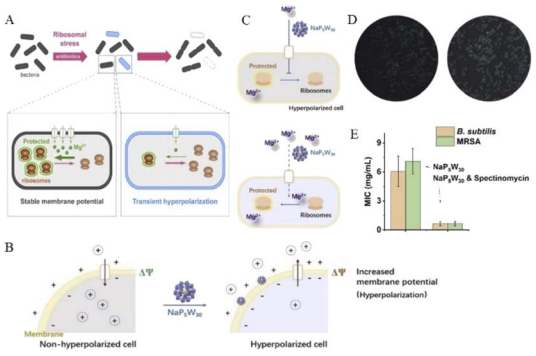

Fig. 14 (A) Schematic diagram of cell hyperpolarization,[3] Copyright 2019, with permission from Cell Press; (B) schematic diagram of NaP_5W_{30} regulating bacterial hyperpolarization and (C) regulating Mg^{2+} in bacteria; (D) ThT fluorescence intensity distribution plots of *Bacillus subtilis* after treatment without (left) and with NaP_5W_{30} (right); (E) MIC of POMs against *B. subtilis* and MRSA in the presence of spectinomycin (2 μg mL^{-1}),[14] Copyright 2021, with permission from Elsevier Inc.

inside the cell. As the cell becomes more negative, more of the ThT dye remains in the cell; thus, the fluorescence of ThT is enhanced. As found from the results, with the increase in extracellular NaP_5W_{30}, the fluorescence intensity of ThT was intensified, indicating that with the presence of more NaP_5W_{30} in the medium, more bacterial cells showed hyperpolarization. However, because the NaP_5W_{30} anion is a highly charged POMs, it has a strong interaction with the cell membrane but does not completely promote its penetration into the cell.[146] Therefore, NaP_5W_{30} may accumulate and interact with the outer membrane of *B. subtilis* cells to induce the accumulation of cations (such as Mg^{2+}) near the outer membrane surface, which leads to a decrease in the cations in *B. subtilis* cells and the increase in intracellular negative charge, resulting in the phenomenon of cell hyperpolarization.

For Mg^{2+} ions, due to their relatively small ionic radius, their hydration shells are thick in aqueous solution. This makes the interaction between them and negatively charged POMs weaker.[147,148] On the contrary, POMs with cavities or pores show reverse-binding affinity for metal cations, and the special trend of divalent cations is $Mg^{2+} > Ca^{2+} > Sr^{2+} > Ba^{2+}$.[149] Different biological systems, whether bacterial or mammalian cells, contain about 20 mM Mg^{2+}.[150] Porous NaP_5W_{30} preferentially capture extracellular free Mg^{2+} due to the high affinity induced by the nanoconfined cavity. To confirm whether porous NaP_5W_{30} induces cell hyperplasia by controlling Mg^{2+}, ThT fluorescence intensity was measured in single bacteria with NaP_5W_{30} and Mg^{2+} in the culture medium. It was confirmed by measurement that adding Mg^{2+} to the growth medium could reduce the proportion of hyperpolarized cells triggered by NaP_5W_{30} (Fig. 14B–D). These results suggest that extracellular NaP_5W_{30} regulates hyperpolarization in *B. subtilis* cells by controlling Mg^{2+}.

Multidrug efflux pumps, proteins that bacteria use to detoxify toxic antibiotics, are thought to have played a key role in the emergence of multidrug-resistant bacteria. Porous POMs macromolecule ions interact with the outer membrane, causing changes in the membrane potential and cell polarity, especially in the phase and morphology of lipid membrane,[151] which will promote the infiltration of intracellular substances targeting antibiotics. Thus, the synergistic application of POMs will promote targeted interactions of antimicrobials and control multidrug resistant bacteria. A combination of NaP_5W_{30} and Spectinomycin was reported for *Bacillus subtilis* and methicillin-resistant *Staphylococcus aureus* (MRSA). The minimum inhibitory concentration (MIC) was found to be approximately 10 times lower when used in combination compared with antibiotics alone (Fig. 14E).

In conclusion, Preyssler-type phosphotungstate NaP_5W_{30} demonstrates that bacterial cells are hyperpolarized by blocking Mg^{2+} transport and reducing Mg^{2+} influx, resulting in ribosomal structural perturbation and bacterial structural instability.[3] NaP_5W_{30} can be used as an effective antibacterial agent in combination with spectinomycin and other conventional antibiotics to control community-prevalent infectious diseases, especially those caused by multidrug-resistant bacteria. In addition, POMs in bacterial control and the required dose of antibiotics were significantly reduced, thus reducing their side effects and selection pressure for clinical use.

4. Challenges and perspectives

Polyoxometalates have rich biocompatibility, structural stability, and modifiability, providing countless possibilities for research in the diagnosis and treatment of cancer as well as antibacterial field, becoming a hot candidate material. In the future, the existing compounds with good performance can be further improved so that they can be put into practical application as soon as possible. For example, POM composite materials presented in this review as MRI contrast agents show better results in animal experiments than commercial contrast agents, which reflects the advantages of the new material; however, it still needs further optimization for practical commercial application in the future. Currently, acidity and GSH concentration in TEM are usually used as the response basis for POMs nanoprobe materials, while other influencing factors are rarely reported. If the influence of other factors is added, it will be of great help to promote the structural renewal and performance improvement of POMs composites. It is also an urgent problem to increase the targeting of POMs to target cells. Since POMs themselves have a certain toxicity, the effect of toxicity on the cells must be considered when complex or pure POMs are released in untargeted cells. These can be wrapped by composite materials to POMs itself or organic modification to reduce toxicity so as to reduce the damage to normal tissues and organs, reduce side effects, and increase safety. On the other hand, current studies focus more on the uptake of POMs or their composite materials by the target cells, while the final metabolic mode and pathway are still unclear, which requires further research. Only when the exact metabolic pathway is known can biosafety be ensured.

In general, the potential tapping of POMs and their nanocomposites for application in cancer and antibacterial materials is in its very beginning, and the future path is promising. In the past few years, new materials have been continuously discovered, and new hopes are forthcoming. Therefore, in the future, this field requires tremendous experimental efforts to elucidate the potential behind POMs and pave the way for next-generation POMs drugs. It is expected that the emergence of new POMs materials will lead to new strategies and schemes in the coming years. Driven by this, we can foresee that future exploration of POM-based materials will continue to deepen and drive further development in this domain.

Author contributions

Dening Chang: investigation, writing-original draft, review. Yanda Li: writing-draft. Yuxuan Chen: writing-draft. Xiaojing Wang: supervision, project administration. Dejin Zang: formal analysis, supervision, writing-review & editing. Teng Liu: conceptualization, resources, supervision, writing-review & editing, project administration.

Conflicts of interest

There are no conflicts to declare.

Acknowledgements

This work was supported by the National Natural Science Foundation of China (21907059), the Shandong Province Chinese Medicine Science and Technology Development Project (M-2022258) and the Academic Promotion Programme of Shandong First Medical University (2019LJ003 and 2019QL011).

Notes and references

1 L. Tang, F. Yu, B. Tang, Z. Yang, W. Fan, M. Zhang, Z. Wang, O. Jacobson, Z. Zhou, L. Li, Y. Liu, D. O. Kiesewetter, W. Tang, L. He, Y. Ma, G. Niu, X. Zhang and X. Chen, *ACS Appl. Mater. Interfaces*, 2019, **11**, 27558–27567.
2 Y. Fang, C. Xing, S. Zhan, M. Zhao, M. Li and H. Liu, *J. Mater. Chem. B*, 2019, **7**, 1933–1944.
3 D. L. Dong-yeon, L. Galera-Laporta, M. Bialecka-Fornal, E. C. Moon, Z. Shen, S. P. Briggs, J. Garcia-Ojalvo and G. M. Süel, *Cell*, 2019, **177**, 352–360.
4 C. Zhang, M. Zhao, H. Zou, X. Zhang and Y. Qi, *J. Inorg. Biochem.*, 2020, **212**, 111212.
5 R. Raza, A. Matin, S. Sarwar, M. Barsukova-Stuckart, M. Ibrahim, U. Kortz and J. Iqbal, *Dalton Trans.*, 2012, **41**, 14329–14336.
6 L. Zong, H. Wu, H. Lin and Y. Chen, *Nano Res.*, 2018, **11**, 4149–4168.
7 Z. Dong, R. Tan, C. Jian, Y. Yang, C. Kong, J. Du, S. Zhu, Y. Zhang, J. Lu and B. Huang, *Eur. J. Med. Chem.*, 2011, **46**, 2477–2484.
8 C. Li, H. Cao, J. Sun, R. Tian, D. Li, Y. Qi, W. Yang and J. Li, *J. Inorg. Biochem.*, 2017, **168**, 67–75.
9 S. Zhou, C. Gu, Z. Li, L. Yang and Z. Zhang, *Appl. Surf. Sci.*, 2019, **498**, 143889.
10 Z. Ma, Y. F. Qiu, H. H. Yang, Y. M. Huang, J. J. Liu, Y. Lu, C. Zhang and P. A. Hu, *ACS Appl. Mater. Interfaces*, 2015, **7**, 22036–22045.
11 S. M. Zhang, H. B. Chen, G. H. Zhang, X. P. Kong, S. Y. Yin, B. Li and L. X. Wu, *J. Mater. Chem. B*, 2018, **6**, 241–248.
12 L. Wang, K. Yu, B. Zhou, Z. H. Su, S. Gao, L. L. Chu and J. R. Liu, *Dalton Trans.*, 2014, **43**, 6070–6078.
13 C. Zhang, W. Bu, D. Ni, C. Zuo, C. Cheng, Q. Li, L. Zhang, Z. Wang and J. Shi, *J Am Chem Soc*, 2016, **138**, 8156–8164.
14 K. Chen, Q. Yu, Y. Liu and P. Yin, *J. Inorg. Biochem.*, 2021, **220**, 111463.
15 J. Ferlay, M. Colombet, I. Soerjomataram, D. M. Parkin, M. Pineros, A. Znaor and F. Bray, *Int. J. Cancer*, 2021, **149**, 778–789.
16 B. Mbage, Y. Li, H. Si, X. Zhang, Y. Li, X. Wang, A. Salah and K. Zhang, *Sens. Actuators, B*, 2020, **304**, 127429.
17 J. Ly, Y. Li, M. N. Vu, B. A. Moffat, K. S. Jack, J. F. Quinn, M. R. Whittaker and T. P. Davis, *Nanoscale*, 2018, **10**, 7270–7280.
18 D. Zang, Y. Huang, Q. Li, Y. Tang and Y. Wei, *Appl. Catal., B*, 2019, **249**, 163–171.
19 Y. Gu, Q. Li, D. Zang, Y. Huang, H. Yu and Y. Wei, *Angew. Chem., Int. Ed.*, 2021, **60**, 13310–13316.
20 A. Bijelic, M. Aureliano and A. Rompel, *Angew. Chem., Int. Ed.*, 2019, **58**, 2980–2999.
21 G. Guedes, S. Wang, H. A. Santos and F. L. Sousa, *Eur. J. Inorg. Chem.*, 2020, **2020**, 2121–2132.
22 J. Gu, L. Zhang, X. Yuan, Y. G. Chen, X. Gao and D. Li, *Bioinorg. Chem. Appl.*, 2018, **2018**, 1–6.
23 A. Bijelic, M. Aureliano and A. Rompel, *Chem. Commun.*, 2018, **54**, 1153–1169.
24 M. Aureliano, N. I. Gumerova, G. Sciortino, E. Garribba, A. Rompel and D. C. Crans, *Coord. Chem. Rev.*, 2021, **447**, 214143.
25 N. Gao, H. Sun, K. Dong, J. Ren, T. Duan, C. Xu and X. Qu, *Nat. Commun.*, 2014, **5**, 1–9.
26 H. Cao, C. Li, Q. Wen, X. Meng, T. Rui, Y. Qi, Y. Wei, J. Li and C. Jamshidkhan, *PLoS One*, 2017, **12**, 0181018.
27 P. Sun, S. Zhang, Z. Xiang, T. Zhao, D. Sun, G. Zhang, M. Chen, K. Guo and X. Xin, *J. Colloid Interface Sci.*, 2019, **547**, 60–68.
28 M. T. Pope and P. D. A. Müller, *Angew. Chem., Int. Ed.*, 2010, **30**, 34–48.
29 B. Li, W. Li, H. Li and L. Wu, *Acc. Chem. Res.*, 2017, **50**, 1391–1399.
30 H. Wang, Y. Yi, B. Li, L. Bi and L. Wu, *Chem.–Eur. J.*, 2011, **17**, 4273–4282.
31 W. Yu, M. Shevtsov, X. Chen and H. Gao, *Chin. Chem. Lett.*, 2020, **31**, 1366–1374.
32 H. Zhang, L. Y. Guo, Z. Xie, X. Xin, D. Sun and S. Yuan, *Langmuir*, 2016, 13736–13745.
33 X. Yan, P. Zhu, J. Fei and J. Li, *Adv. Mater.*, 2010, **22**, 1283–1287.
34 K. Stroobants, G. Absillis, E. Moelants, P. Proost and T. N. Parac-Vogt, *Chem.–Eur. J.*, 2014, **20**, 3894–3897.
35 M. Aureliano, N. I. Gumerova, G. Sciortino, E. Garribba, C. C. McLauchlan, A. Rompel and D. C. Crans, *Coord. Chem. Rev.*, 2022, **454**, 214344.
36 S. She, S. Bian, J. Hao, J. Zhang, J. Zhang and Y. Wei, *Chem.–Eur. J.*, 2014, **20**, 16987–16994.
37 S. She, S. Bian, R. Huo, K. Chen, Z. Huang, J. Zhang, J. Hao and Y. Wei, *Sci. Rep.*, 2016, **6**, 33529.
38 Y. Gu, Q. Li, Y. Huang, Y. Zhu, Y. Wei and L. Ruhlmann, *Chem. Commun.*, 2020, **56**, 2869–2872.
39 S. Nussbaumer, P. Bonnabry, J. L. Veuthey and S. Fleury-Souverain, *Talanta*, 2011, **85**, 2265–2289.
40 J. Barretina, G. Caponigro, N. Stransky, K. Venkatesan and E. Al, *Natur*, 2012, **483**, 603–607.
41 K. P. Carter, A. M. Young and A. E. Palmer, *Chem. Rev.*, 2014, **114**, 4564–4601.
42 H. Zhao, H. Wang, H. Li, T. Zhang, J. Zhang, W. Guo, K. Fu and G. Du, *Nanoscale Adv.*, 2022, **4**, 1815–1826.
43 J. Hong, D. A. Heller, M. Kalbacova, J. H. Kim and M. S. Strano, *Nat. Nanotechnol.*, 2010, **5**, 302–309.
44 L. M. Yang, N. Yang, W. Li, Z. Pan, B. Yu and B. Tang, *Anal. Chem.*, 2015, **87**, 3678–3684.

45 B. Giuseppina, G. Fabrizio, P. Stefania, C. Rosa, D. Martina, A. Alessia, C. Giovanni, L. Alessio, F. Carlo and D. Chiara, *Antioxidants*, 2016, **5**, 7.
46 E. Noch, L. Palma, I. Yim, D. Barnett, B. BHinder, E. Benedetti, J. Krumsiek, O. Elemento and L. Cantley, *Neuro-Oncol.*, 2021, **23**, 33–34.
47 N. Gan, P. Xiong, J. Wang, T. Li, F. Hu, Y. Cao and L. Zheng, *J. Anal. Methods Chem.*, 2013, **2013**, 482316.
48 J. Wang, D. Han, X. Wang, B. Qi and M. Zhao, *Biosens. Bioelectron.*, 2012, **36**, 18–21.
49 Z. Sun, H.-Z. Bie, M.-J. Wei, J.-J. Wang, X.-G. Mi, X.-H. Wang and Y. Wu, *Chin. Chem. Lett.*, 2013, **24**, 76–78.
50 J. Wang, X. Mi, H. Guan, X. Wang and Y. Wu, *Chem. Commun.*, 2011, **47**, 2940–2942.
51 Y. Ji, J. Xu, X. Chen, L. Han, X. Wang, F. Chai and M. Zhao, *Sens. Actuators, B*, 2015, **208**, 497–504.
52 X. Li, L. Sun, X. Yang, K. Zhou, G. Zhang, Z. Tong, C. Wang and J. Sha, *Analyst*, 2019, **144**, 3347–3356.
53 A. Fraternale, S. Brundu and M. Magnani, *Biol. Chem.*, 2017, **398**, 261–275.
54 N. Traverso, R. Ricciarelli, M. Nitti, B. Marengo, A. L. Furfaro, M. A. Pronzato, U. M. Marinari and C. Domenicotti, *Oxid. Med. Cell. Longevity*, 2013, **2013**, 972913.
55 T. Ishimoto, O. Nagano, T. Yae, M. Tamada, T. Motohara, H. Oshima, M. Oshima, T. Ikeda, R. Asaba, H. Yagi, T. Masuko, T. Shimizu, T. Ishikawa, K. Kai, E. Takahashi, Y. Imamura, Y. Baba, M. Ohmura, M. Suematsu, H. Baba and H. Saya, *Cancer Cell*, 2011, **19**, 387–400.
56 A. Babakhanian, S. Kaki, M. Ahmadi, H. Ehzari and A. Pashabadi, *Biosens. Bioelectron.*, 2014, **60**, 185–190.
57 N. Cheng, D. Du, X. Wang, D. Liu, W. Xu, Y. Luo and Y. Lin, *Trends Biotechnol.*, 2019, **37**, 1236–1254.
58 C. Sun, X. Chen, J. Xu, M. Wei, J. Wang, X. Mi, X. Wang, Y. Wu and Y. Liu, *J. Mater. Chem. A*, 2013, **1**, 4699–4705.
59 S. Zhong, H. Z. Bie, M. J. Wei, J. J. Wang, X. G. Mi, X. H. Wang and Y. Wu, *Chin. Chem. Lett.*, 2013, **24**, 76–78.
60 H. R. Moorman, D. Poschel, J. D. Klement, C. Lu and K. Liu, *Cancers*, 2020, **12**, 3379.
61 E. R. Gimba, M. Brum and G. Nestal De Moraes, *Int. J. Oncol.*, 2019, **54**, 420–430.
62 A. Sinha, H. Zhao, Y. Huang, X. Lu, J. Chen and R. Jain, *TrAC, Trends Anal. Chem.*, 2018, **105**, 424–435.
63 N. Alegret, A. Dominguez-Alfaro, J. M. González-Domínguez, B. Arnaiz, U. Cossío, S. Bosi, E. Vázquez, P. Ramos-Cabrer, D. Mecerreyes and M. Prato, *ACS Appl. Mater. Interfaces*, 2018, **10**, 43904–43914.
64 D. Ni, D. Jiang, H. F. Valdovinos, E. B. Ehlerding, B. Yu, T. E. Barnhart, P. Huang and W. Cai, *Nano Lett.*, 2017, **17**, 3282–3289.
65 G. Liu, J. Zhu, H. Guo, A. Sun, P. Chen, L. Xi, W. Huang, X. Song and X. Dong, *Angew. Chem., Int. Ed. Engl.*, 2019, **58**, 18641–18646.
66 H. Wu, M. Zhi, C. Chen, Y. Zhu, P. Ma, J. Wang and J. Niu, *Dalton Trans.*, 2019, **48**, 13850–13857.
67 A. C. Venu, R. Nasser Din, T. Rudszuck, P. Picchetti, P. Chakraborty, A. K. Powell, S. Kramer, G. Guthausen and M. Ibrahim, *Molecules*, 2021, **26**, 7481.
68 D. Ni, D. Jiang, H. J. Im, H. F. Valdovinos, B. Yu, S. Goel, T. E. Barnhart, P. Huang and W. Cai, *Biomaterials*, 2018, **171**, 144–152.
69 S. Kunjachan, J. Ehling, G. Storm, F. Kiessling and T. Lammers, *Chem. Rev.*, 2015, **115**, 10907–10937.
70 J. N. Liu, W. B. Bu and J. L. Shi, *Chem. Rev.*, 2017, **117**, 6160–6224.
71 C. Liu, C. Li, S. Jiang, C. Zhang and Y. Tian, *Nanoscale Adv.*, 2022, **4**, 173–181.
72 K. N. Raymond and V. C. Pierre, *Bioconjugate Chem.*, 2005, **16**, 3–8.
73 R. V. Roosbroeck, W. V. Roy, T. Stakenborg, J. Trekker, A. D'Hollander, T. Dresselaers, U. Himmelreich, J. Lammertyn and L. Lagae, *Acs Nano*, 2014, **8**, 2269–2278.
74 S. Laurent, D. Forge, M. Port, A. Roch, C. Robic, L. V. Elst and R. N. Muller, *Chem. Rev.*, 2010, **110**, 2574.
75 Z.-X. Chang, C.-H. Li, Y.-C. Chang, C.-Y. F. Huang, M.-H. Chan and M. Hsiao, *Nanoscale Adv.*, 2022, **4**, 377–386.
76 A. Narmani, B. Farhood, H. Haghi-Aminjan, T. Mortezazadeh, A. Aliasgharzadeh, M. Mohseni and M. Najafi, *J. Drug Delivery Sci. Technol.*, 2018, **44**, 457–466.
77 E. Terreno, D. Castelli, A. Viale and S. Aime, *Chem. Rev.*, 2010, **110**, 3019–3042.
78 J. Feng, G. Sun, F. Pei and M. Liu, *J. Inorg. Biochem.*, 2002, **92**, 193–199.
79 J. Feng, X. Li, F. Pei, G. Sun and M. Liu, *Magn. Reson. Imaging*, 2002, **20**, 407–412.
80 Z. Li, W. Li, X. Li, F. Pei, Y. Li and L. Hao, *Magn. Reson. Imaging*, 2007, **25**, 412–417.
81 L. S. Luan, L. Qi, L. Zhao, N. N. Li and Z. H. Li, *Prog. Polym. Sci.*, 2016, **58**, 1–26.
82 J. Ly, Y. Li, M. N. Vu, B. A. Moffat, K. S. Jack, J. F. Quinn, M. R. Whittaker and T. P. Davis, *Nanoscale*, 2018, **10**, 7270–7280.
83 Y. Wang, S. Zhou, D. Kong, H. Yang, W. Chai, U. Kortz and L. Wu, *Dalton Trans.*, 2012, **41**, 10052–10059.
84 S. Zhang, M. Li, Y. Zhang, R. Wang, Y. Song, W. Zhao and S. Lin, *Dalton Trans.*, 2021, **50**, 8076–8083.
85 J. Chen, C. Ning, Z. Zhou, P. Yu, Y. Zhu, G. Tan and C. Mao, *Prog. Mater. Sci.*, 2019, **99**, 1–26.
86 N. Ogiwara, T. Iwano, T. Ito and S. Uchida, *Coord. Chem. Rev.*, 2022, **462**, 214524.
87 W. Xu, D. Ren, Z. Yu, J. Hou, F. Huang, T. Gan, P. Ji, C. Zhang, L. Ma and Y. Hu, *Nanoscale Adv.*, 2022, **4**, 1577–1586.
88 L. Cheng, C. Wang, L. Z. Feng, K. Yang and Z. Liu, *Chem. Rev.*, 2014, **114**, 10869–10939.
89 K. Yang, L. Z. Feng, X. Z. Shi and Z. Liu, *Chem. Soc. Rev.*, 2013, **42**, 530–547.
90 B. Nikoobakht and M. A. El-Sayed, *Chem. Mater.*, 2003, **15**, 1957–1962.
91 Y. Xia, W. Li, C. M. Cobley, J. Chen, X. Xia, Q. Zhang, M. Yang, E. C. Cho and P. K. Brown, *Acc. Chem. Res.*, 2011, **44**, 914–924.

92 K. Yang, H. Xu, L. Cheng, C. Y. Sun, J. Wang and Z. Liu, *Adv. Mater.*, 2012, **24**, 5586–5592.
93 L. Cheng, K. Yang, Q. Chen and Z. Liu, *ACS Nano*, 2012, **6**, 5605–5613.
94 L. Cheng, W. W. He, H. Gong, C. Wang, Q. Chen, Z. P. Cheng and Z. Liu, *Adv. Funct. Mater.*, 2013, **23**, 5893–5902.
95 S. R. Rao, A. E. Snaith, D. Marino, X. Cheng, S. T. Lwin, I. R. Orriss, F. C. Hamdy and C. M. Edwards, *Br. J. Cancer*, 2017, **116**, 227–236.
96 J. Iqbal, M. I. El-Gamal, S. A. Ejaz, J. Lecka, J. Sévigny and C.-H. Oh, *J. Enzyme Inhib. Med. Chem.*, 2018, **33**, 479–484.
97 L. C. Huan, C. V. Phuong, L. C. Truc, V. N. Thanh, H. Huong, N. T. Thuan, E. J. Park, A. Y. Ji and J. S. Kang, *J. Enzyme Inhib. Med. Chem.*, 2019, **34**, 465–478.
98 L. Firoozpour, L. Gao, S. Moghimi, P. Pasalar, J. Davoodi, M.-W. Wang, Z. Rezaei, A. Dadgar, H. Yahyavi and M. Amanlou, *J. Enzyme Inhib. Med. Chem.*, 2020, **35**, 1674–1684.
99 K. M. Regula, K. Ens and L. A. Kirshenbaum, *J. Mol. Cell. Cardiol.*, 2003, **35**, 559–567.
100 J. T. Hwang, D. Y. Kwon, O. J. Park and M. S. Kim, *Genes Nutr.*, 2008, **2**, 323–326.
101 L. Xerri, F. Palmerini, E. Devilard, T. Defrance and F. Birg, *J. Pathol.*, 2015, **192**, 194–202.
102 M. Maher, A. E. Kassab, A. F. Zaher and Z. Mahmoud, *J. Enzyme Inhib. Med. Chem.*, 2019, **34**, 532–546.
103 M. A. Sanz, D. Grimwade, M. Tallman, B. Löwenberg, P. Fenaux, E. Estey, T. Naoe, E. Lengfelder, T. Büchner and H. Döhner, *Blood*, 2008, **113**, 1875–1891.
104 J. R. Davie and D. N. Chadee, *J. Cell. Biochem.*, 2015, **72**, 203–213.
105 J. Ruzzolini, A. Laurenzana, E. Andreucci, S. Peppicelli, F. Bianchini, F. Carta, C. T. Supuran, M. N. Romanelli, C. Nediani and L. Calorini, *J. Enzyme Inhib. Med. Chem.*, 2020, **35**, 391–397.
106 A. Ruijter, A. Gennip, H. N. Caron, S. Kemp and A. Kuilenburg, *Biochem. J.*, 2003, **370**, 737–749.
107 S. Nencetti, D. Cuffaro, E. Nuti, L. Ciccone, A. Rossello, M. Fabbi, F. Ballante, G. Ortore, G. Carbotti and F. Campelli, *J. Enzyme Inhib. Med. Chem.*, 2021, **36**, 34–47.
108 H. R. Kim, E. J. Kim, S. H. Yang, E. T. Jeong, C. Park, J. H. Lee, M. J. Youn, H. S. So and R. Park, *Exp. Mol. Med.*, 2006, **38**, 616–624.
109 B. Hamandi, S. Husain, A. Humar and E. A. Papadimitropoulos, *Clin. Infect. Dis.*, 2014, **59**, 1074–1082.
110 K. E. Jones, N. G. Patel, M. A. Levy, A. Storeygard, D. Balk, J. L. Gittleman and P. Da Szak, *Natur*, 2008, **451**, 990–993.
111 F. Nederberg, Y. Zhang, J. Tan, K. Xu, H. Wang, C. Yang, S. Gao, X. D. Guo, K. Fukushima and L. Li, *Nat. Chem.*, 2011, **3**, 409–414.
112 M. A. Kohanski, D. J. Dwyer, B. Hayete, C. A. Lawrence and J. J. Collins, *Cell*, 2007, **130**, 797–810.
113 D. Feldman, *J. Macromol. Sci., Part A: Pure Appl.Chem.*, 2016, **53**, 55–62.
114 Q. Pena, A. Wang, O. Zaremba, Y. Shi, H. W. Scheeren, J. M. Metselaar, F. Kiessling, R. M. Pallares, S. Wuttke and T. Lammers, *Chem. Soc. Rev.*, 2022, **51**, 2544–2582.
115 F. Watari, N. Takashi, A. Yokoyama, M. Uo, T. Akasaka, Y. Sato, S. Abe, Y. Totsuka and K. Tohji, *J. R. Soc., Interface*, 2009, **6**, 371–388.
116 T. Zhao, S. Zhang, Y. Bi, D. Sun, F. Kong, Z. Yuan and X. Xin, *Colloids Surf., A*, 2020, **603**, 125257.
117 Y. Fang, T. Liu, C. Xing, J. Chang and M. Li, *Int. J. Pharm.*, 2020, **591**, 119990.
118 A. Umapathi, N. P. Nagaraju, H. Madhyastha, D. Jain, S. P. Srinivas, V. M. Rotello and H. K. Daima, *Colloids Surf., B*, 2019, **184**, 110522.
119 M. R. Olsen, I. Colliard, T. Rahman, T. C. Miyaishi, B. Harper, S. Harper and M. Nyman, *ACS Appl. Mater. Interfaces*, 2021, **13**, 19497–19506.
120 X. Wei, K. Ma, Y. Cheng, L. Sun, D. Chen, X. Zhao, H. Lu, B. Song, K. Yang and P. Jia, *ACS Appl. Polym. Mater.*, 2020, **2**, 2541–2549.
121 S. Zhang, B. Peng, P. Xue, X. Kong, Y. Tang, L. Wu and S. Lin, *Soft Matter*, 2019, **15**, 5375–5379.
122 C. Zhang, M. Zhao, H. Zou, X. Zhang, R. Sheng, Y. Zhang, B. Zhang, C. Li and Y. Qi, *J. Inorg. Biochem.*, 2020, **212**, 111212.
123 K. H. Wu, Y. C. Chang and J. C. Wang, *J. Inorg. Biochem.*, 2019, **199**, 110788.
124 Q. Li, Y. Zhang, X. Huang, D. Yang, L. Weng, C. Ou, X. Song and X. Dong, *Chem. Eng. J.*, 2021, **407**, 127200.
125 Y. Fang, C. Xing, J. Liu, Y. Zhang, M. Li and Q. Han, *Int. J. Biol. Macromol.*, 2020, **154**, 732–738.
126 G.-Z. Shen, G.-H. Zou, H.-Y. Li and Y.-L. Zou, *J. Mol. Struct.*, 2019, **1198**, 126831.
127 B. Fan, N. Cui, Z. Xu, K. Chen, P. Yin, K. Yue and W. Tang, *Biomacromolecules*, 2022, **23**, 972–982.
128 C. Xing, P. Ma, M. Zhao, J. Chang, X. Guo, L. Sun and M. Li, *CrystEngComm*, 2021, **23**, 3919–3928.
129 T. Ma, P. Yang, I. Dammann, Z. Lin, A. S. Mougharbel, M. X. Li, F. Adascalitei, R. Mitea, C. Silvestru, C. Thorstenson, M. S. Ullrich, K. Cseh, M. A. Jakupec, B. K. Keppler, M. Donalisio, R. Cavalli, D. Lembo and U. Kortz, *Inorg. Chem.*, 2020, **59**, 2978–2987.
130 K. Riku, S. Yoshihiro, K. Kiyofumi, M. Sadaatsu, S. Mukai and S. Sawada, *Angew. Chem., Int. Ed.*, 2016, **55**, 11377–11381.
131 G. Rui, X. Ge, M. Li, X. Lin, D. D. Liu, D. Wang, S. Y. Li and B. Li, *ACS Appl. Mater. Interfaces*, 2016, **8**, 22942–22952.
132 C. Yang, W. Guo, L. Cui, N. An, T. Zhang, G. Guo, H. Lin and F. Qu, *J. Mater. Chem. B*, 2015, **3**, 1010–1019.
133 L. S. Lin, Z. X. Cong, J. B. Cao, K. M. Ke, Q. L. Peng, J. H. Gao, H. H. Yang, G. Liu and X. Y. Chen, *Acs Nano*, 2014, **8**, 3876–3883.
134 M. Wu, Y. Li, R. Yue, X. Zhang and Y. Huang, *Sci. Rep.*, 2017, **7**, 1–9.
135 Y. Hu, Y. Zhou, N. Zhao, F. Liu and F. J. Xu, *Small*, 2016, **12**, 2459–2468.
136 B. Shang, Y. Wang, B. Peng and Z. Deng, *Appl. Surf. Sci.*, 2020, **509**, 145360.

137 L. Guo, Q. Liu, G. Li, J. Shi, J. Liu, T. Wang and G. Jiang, *Nanoscale*, 2012, **4**, 5864–5867.
138 Z. Rong, P. F. Ren, H. C. Yang and Z. K. Xu, *J. Membr. Sci.*, 2014, **466**, 18–25.
139 M. Aureliano, *Oxid. Med. Cell. Longevity*, 2016, **2016**, 1–8.
140 S. Soares, H. Martins, R. O. Duarte, J. J. Moura, J. Coucelo, C. Gutiérrez-Merino and M. Aureliano, *J. Inorg. Biochem.*, 2007, **101**, 80–88.
141 S. Liu, T. H. Zeng, M. Hofmann, E. Burcombe, J. Wei, R. Jiang, J. Kong and Y. Chen, *Acs Nano*, 2011, **5**, 6971–6980.
142 P. Sami, T. D. Anand, M. Premanathan and K. Rajasekaran, *Transition Met. Chem.*, 2010, **35**, 1019–1025.
143 H. S. Kafil and A. M. Mobarez, *Open Microbiol. J.*, 2015, **9**, 14.
144 B. D. Glisic, L. Senerovic, P. Comba, H. Wadepohl, A. Veselinovic, D. R. Milivojevic, M. I. Djuran and J. Nikodinovic-Runic, *J. Inorg. Biochem.*, 2016, **155**, 115–128.
145 Y. Chu, J. Chen, F. Haso, Y. Gao, J. E. Szymanowski, P. C. Burns and T. Liu, *Chem.–Eur. J.*, 2018, **24**, 5479–5483.
146 B. Chakraborty, G. Gan-Or, M. Raula, E. Gadot and I. A. Weinstock, *Nat. Commun.*, 2018, **9**, 1–8.
147 A. Misra, K. Kozma, C. Streb and M. Nyman, *Angew. Chem., Int. Ed.*, 2020, **59**, 596–612.
148 S. Abdelhameed, L. Vandebroek, F. D. Azambuja and T. N. Parac-Vogt, *Inorg. Chem.*, 2020, **59**, 10569–10577.
149 J. A. Fernández, X. López, C. Bo, C. de Graaf, E. J. Baerends and J. M. Poblet, *J. Am. Chem. Soc.*, 2007, **129**, 12244–12253.
150 J. M. Pigga, J. A. Teprovich Jr, R. A. Flowers, M. R. Antonio and T. Liu, *Langmuir*, 2010, **26**, 9449–9456.
151 L. Piddock, *Nat. Rev. Microbiol.*, 2006, **4**, 629–636.